

POLITECNICO OF TORINO

Master's Degree in Energy and Nuclear Engineering



**Politecnico
di Torino**

Master's Degree Thesis

Design of the Gearbox of a 22 MW Offshore Wind Turbine

Supervisors

Prof. Giovanni BRACCO

Prof. Amir NEJAD

Candidate

Aurora PIZZINAT 301642

29 November 2023

Abstract

In a world where the climate crisis is the dominating topic discussed all over the news and the internet, the necessity of developing new renewable technologies to keep up the progress while fighting global warming seems fundamental. Being carbon-free and simultaneously satisfying the energy demands of billions of people worldwide is one of science's biggest challenges. Sometimes, it is not just a matter of finding something new but of improving what already exists, and that is the direction taken by this master's thesis. Wind turbines are energy systems that have existed since ancient times, with different purposes from today, but still, they were highly used. After several centuries of being substituted by fossil fuels, they become one of the most critical renewable technologies able to satisfy several demands at the same time. It is known that the latest wind turbine studied and designed is the 15 MW offshore wind turbine, but in early 2023, the necessity to have something more drives towards a 22 MW wind turbine. The design of this specific system is still at the beginning, and further development will be added in the following years before being commercialized. For now, the work is based on the design and, mostly, on the sizing of the turbine gearbox. Starting with the choice of the location where this hypothetical wind turbine could be placed, which specifically for this thesis is 9 km from the shore of the city of Bergen, Norway, the global analysis is carried out by using peculiar software such as OpenFAST. Wind data (torque and the Weibull wind speed distribution) are gathered, followed by the LDD and ultimate strength analysis. The initial configuration of the gearbox is then selected: a medium-speed gearbox with three planetary stages to have a more compact design while keeping the efficiency high. The first and the secondary stages are designed in KISSsoft with five planets due to the enormous torque they have to face, even though at the end of the work it is observed that probably seven planets for the first stage would have been a better solution to decrease the weight of the device while keeping still the other results. The third stage has three planets and a helix angle lower than the first two stages to decrease the axial loads. After finding the optimal solution for the gears of each stage, bearings and shafts are then designed in KISSsoft, a design software used to size, analyze, and optimize machine elements and gearboxes. While the gears are designed according to both LDD and Ultimate strength analysis, the bearings' design is based on the fatigue analysis. The final and optimal configuration is selected according to the rating life and the safety factor of the bearings, keeping in mind that having a machine working for such a high power would lead to an overdesigned condition, mainly when it comes to the bearings of the last stage. Further studies and optimization analysis will be carried out to make the device ready to be commercialized sooner.

Abstract

In un mondo in cui la crisi climatica è uno degli argomenti predominanti presente nei notiziari e in internet, la necessità di sviluppare nuove tecnologie rinnovabili per sostenere il progresso, combattendo nel frattempo contro il riscaldamento globale, sembra fondamentale. Essere senza emissioni di carbonio e contemporaneamente soddisfare le esigenze energetiche di miliardi di persone in tutto il mondo, è una delle più grandi sfide che la scienza e l'ingegneria devono affrontare. A volte, non è solo una questione di realizzare qualcosa di nuovo, ma di migliorare ciò che già esiste, e questa è la direzione presa dalla seguente tesi. Le turbine eoliche sono sistemi energetici che esistono fin dai tempi antichi, con scopi diversi da oggi, ma ancora, ampiamente utilizzate. Dopo diversi secoli in cui i combustibili fossili hanno predominato su scala mondiale, le turbine eoliche diventano una delle tecnologie rinnovabili più critiche in grado di soddisfare allo stesso tempo diverse richieste. L'ultima turbina eolica studiata e progettata risulta essere la turbina eolica offshore da 15 MW, ma a partire dal 2023, la necessità di qualcosa di più potente, spinge verso una turbina eolica da 22 MW. Il design di questo sistema specifico è ancora all'inizio, e ulteriori sviluppi saranno aggiunti negli anni successivi, prima di essere commercializzato. Per ora, il lavoro si basa su il design e, soprattutto, sul dimensionamento del gearbox. A partire dalla scelta del luogo in cui questa ipotetica turbina eolica potrebbe essere collocata, che specificamente per questa tesi è a 9 km dalle coste della città di Bergen, Norvegia, viene effettuata un'analisi globale attraverso specifici software, come OpenFAST. I dati del vento (coppia e distribuzione della velocità del vento secondo la distribuzione di Weibull) sono raccolti, seguiti dall'LDD e dall'ultimate strength analysis. È di conseguenza possibile selezionare la configurazione iniziale del gearbox: un gearbox a media velocità con tre stadi planetari per avere un design più compatto, mantenendo allo stesso tempo alta l'efficienza. Il primo e il secondo stadio sono progettati in KISSsoft con cinque pianeti a causa dell'enorme coppia che sono soggetti, anche se alla fine del lavoro si può osservare come probabilmente un design con sette pianeti per il primo stadio risulterebbe una soluzione migliore per diminuire il peso del dispositivo mantenendo costanti gli altri risultati. Il terzo stadio ha tre pianeti e un helix angle inferiore ai primi due stadi in modo da diminuire i carichi assiali. Dopo aver trovato la soluzione ottimale per le ruote dentate di ogni fase, i cuscinetti e gli alberi vengono quindi progettati in KISSsoft, un software di progettazione utilizzato per dimensionare, analizzare e ottimizzare gli elementi della macchina e le scatole degli ingranaggi. Mentre le ruote dentate sono progettate in base alla LDD analysis e Ultimate Strength analysis, il dimensionamento dei cuscinetti si basa unicamente sull'analisi di fatica. La configurazione finale e ottimale viene selezionata in base al

rating life e al fattore di sicurezza dei cuscinetti, tenendo presente che avere una macchina che lavora per una potenza così elevata potrebbe portare a una condizione di sovradimensionamento, specialmente per quelli dell'ultima fase. Ulteriori studi e analisi di ottimizzazione saranno effettuati per rendere il dispositivo pronto per essere commercializzato il prima possibile.

Abstract

I en verden der klimakrisen er det dominerende temaet i nyhetsbildet og på internett, er det helt nødvendig å utvikle ny fornybar teknologi for å holde fremdriften og samtidig bekjempe den globale oppvarmingen. Å være karbonfri og samtidig dekke energibehovet til milliarder av mennesker verden over er en av vitenskapens største utfordringer. Noen ganger handler det ikke bare om å finne noe nytt, men om å forbedre det som allerede finnes, og det er i den retningen denne masteroppgaven går. Vindturbiner er energisystemer som har eksistert siden antikken, med andre formål enn i dag, men som likevel har vært mye brukt. Etter å ha blitt erstattet av fossilt brensel i flere århundrer, har de blitt en av de viktigste fornybare teknologiene som kan tilfredsstille flere behov samtidig. Som kjent er den nyeste vindturbinen som er studert og designet, en 15 MW offshore-vindturbin, men i begynnelsen av 2023 vil behovet for å ha noe mer føre til en 22 MW-vindturbin. Utformingen av dette spesifikke systemet er fortsatt i startfasen, og det vil bli videreutviklet i løpet av de neste årene før det kommersialiseres. Foreløpig er arbeidet basert på design og, for det meste, på dimensjonering av turbinens girkasse. Med utgangspunkt i valget av stedet der denne hypotetiske vindturbinen kan plasseres, som spesifikt for denne oppgaven er 9 km fra kysten av Bergen, utføres den globale analysen ved hjelp av programvare som OpenFAST. Vinddata (dreiemoment og Weibull vindhastighetsfordeling) samles inn, etterfulgt av LDD og bruddstyrkeanalyse. Deretter velges den opprinnelige konfigurasjonen av girkassen: en girkasse med middels hastighet og tre planettrinn for å få en mer kompakt design samtidig som effektiviteten holdes høy. Det første og det andre trinnet er konstruert i KISSsoft med fem planeter på grunn av det enorme dreiemomentet de må håndtere, selv om det mot slutten av arbeidet viser seg at syv planeter for det første trinnet sannsynligvis hadde vært en bedre løsning for å redusere vekten på enheten og samtidig beholde de andre resultatene. Det tredje trinnet har tre planeter og en lavere helixvinkel enn de to første trinnene for å redusere de aksiale belastningene. Etter å ha funnet den optimale løsningen for tannhjulene i hvert trinn, blir lagrene og akslene designet i KISSsoft, en designprogramvare som brukes til å dimensjonere, analysere og optimalisere maskinelementer og girkasser. Mens tannhjulene designes i henhold til både LDD- og ultimate styrkeanalyse, er lagrenes design basert på utmattingsanalyse. Den endelige og optimale konfigurasjonen velges i henhold til lagrenes nominelle levetid og sikkerhetsfaktor, med tanke på at en maskin som arbeider med så høy effekt vil føre til en overdesignet tilstand, hovedsakelig når det gjelder lagrene i det siste trinnet. Ytterligere studier og optimaliseringsanalyser vil bli utført for å gjøre enheten klar til å bli kommersialisert raskere.

Acknowledgements

29th November 2023 marks the end of an important chapter in my university career, and therefore, I would like to offer my thanks to all those who have been a part of it.

Un ringraziamento particolare al Professore Giovanni Bracco per essermi stato accanto in questo percorso e avermi dato la possibilità di svolgere parte del mio lavoro in Norvegia.

En stor takk til professor Amir Nejad, medopponent for avhandlingen, for hans konstante støtte, uunnværlige tips og medvirkning i arbeidet med hvert kapittel i avhandlingen, Ashkan Rezaei and Jakob Vincent Gebel for the valuable advice and help given to me during the development of my thesis.

I would like to thank NTNU for giving me the opportunity to do my thesis work in an interesting and dynamic place, which allowed me to get involved and gain experience that will be valuable for my future.

Ai miei genitori per essermi stati accanto e supportata in ogni mia decisione.

Ai miei nonni e zii un profondo ringraziamento per avermi sostenuta durante questo percorso.

Ai miei amici e miei colleghi di università e a tutti quelli che hanno incrociato la loro vita con la mia lasciandomi qualcosa di buono.

Aurora Pizzinat, Politecnico di Torino

Table of Contents

List of Tables	VII
List of Figures	VIII
Acronyms	XI
1 Introduction	1
1.1 Motivation	1
1.2 Objective	3
1.3 History and developement	4
1.4 Structure of the thesis	5
2 Literature Review	7
2.1 State of art of wind turbine	7
2.1.1 Classification	7
2.1.2 Wind turbine main components	9
2.1.3 The drivetrain	10
2.2 Wind turbine Aerodynamic	11
2.2.1 The wind	11
2.2.2 Aerodynamic forces: lift and drag	12
2.2.3 Stall condition	14
2.3 BEM method for wind turbine	15
2.3.1 Prantl's tip loss factor	19
2.3.2 Glauert correction	20
2.3.3 Unsteady BEM model	20
2.4 DSL - Design Standard Requirements	20
2.4.1 IEC 61400-1	20
2.4.2 IEC 61400-3	21
2.5 Design tools for an offshore wind turbine	22

3	Global Analysis for the 22MW Wind Turbine	23
3.1	Location definition	23
3.2	22 MW wind turbine	25
3.3	Design Load Cases and Global Analysis for the 22 MW turbine . .	26
4	Local Analysis for the 22MW Wind Turbine	29
4.1	Drivetrain configuration for the 22 MW offshore wind turbine . . .	29
4.2	The Gearbox	30
4.2.1	Gears	32
4.2.2	Bearings and Shafts	35
5	Results and Discussion	38
5.1	Global Analysis results	38
5.1.1	Global Analysis: Location definition Outcomes	38
5.1.2	Global Analysis: Design Load Cases Outcomes	40
5.2	Local Analysis results	41
5.2.1	Local Analysis: Gears Outcomes	42
5.2.2	Local Analysis: Shaft and Bearing Outcomes	46
6	Conclusion	49
A	Appendix A	51
A.1	Wind turbine Siting	51
A.2	Global Analysis	55
A.3	Local Analysis	61
	Bibliography	68

List of Tables

2.1	Basic parameters for wind turbine classes.	21
2.2	Example of Design Load Cases defined in EIC 61400-3.	22
3.1	Characteristic of the location where the turbine is supposed to be installed.	24
3.2	DLC for the 22 MW wind turbine main features.	26
4.1	22MW reference gearbox specification.	32
4.2	Gear's face width and weight variation due to different helix angle.	33
5.1	Stage 1, gears main parameters obtained from Fatigue and Ultimate Strength analysis.	43
5.2	Stage 2, gears main parameters obtained from Fatigue and Ultimate Strength analysis.	44
5.3	Stage 3, gears main parameters obtained from Fatigue and Ultimate Strength analysis.	46
5.4	Stage 3, gears main parameters when the helix angle is equal to 4°	46
A.1	Specification for stage 1, gears.	61
A.2	Specification for stage 2, gears.	62
A.3	Specification for stage 3, gears.. . . .	63
A.4	Stage 3 and Helix angle equal to 4°, specifications from LDD analysis.	64
A.5	Stage 1, bearings specification.	65
A.6	Stage 2, bearings specification.	65
A.7	Stage 3, bearings specification.	66

List of Figures

1.1	Final energy consumption by sector, EU, 1990-2021, Terajoules (TJ)	2
1.2	Imports of selected energy products, EU, 1990-2021 Petajoule (PJ).	3
1.3	Wind turbines at sea. Author: CGP Grey. License: Creative Commons, Attribution 2.0 Generic.	4
1.4	Flow chart of the structure of the thesis.	6
2.1	Vertical and Horizontal axis wind turbine, arborwind.com	8
2.2	Wind turbine structure, sustainablesolutions.duke-energy.com	9
2.3	Drivetrain structure, Qian, P., Ma, X., and Zhang, D. Estimating Health Condition of the Wind Turbine Drivetrain System	10
2.4	Pressure gradient between upper and bottom part of a body	13
2.5	Stall condition	15
2.6	Velocities at the rotor plane	17
2.7	Local loads on the blade	18
3.1	22MW Wind Turbine Location from Google Earth	24
3.2	Weibull Wind speed distribution for the chosen location.	25
3.3	LDD for the the $18 \frac{m}{s}$ wind speed.	27
3.4	LDD for the whole wind speed range.	28
4.1	Three-point (top) and four-point (bottom) suspension drive train. Y. Guo, T. Parsons, K. Dykes, R.N. King: A systems engineering analysis of three-point and four-point wind turbine drivetrain configurations	30
4.2	Gearbox configuration, with three planetary stages	31
4.3	Planet gear's bearings configuration from KISSsoft, stage 1.	36
4.4	Sun gear's bearings configuration from KISSsoft, stage 1.	37
5.1	Occurrence of Wind Speed from Matlab	39
5.2	average sea state as a function of wind speed from Matlab	39
5.3	12 m/s Rotor Speed and Torque as time function	40

5.4	22 m/s Rotor Speed Resonance	41
5.5	Planet-sun gear meshing and the planet-ring meshing, stage 1, from KISSsoft	42
5.6	2-D configuration of stage 1 from KISSsoft	42
5.7	Planet-sun gear meshing and the planet-ring meshing, stage 2, from KISSsoft	43
5.8	2-D configuration of stage 2 from KISSsoft	44
5.9	Planet-sun gear meshing and the planet-ring meshing, stage 3, from KISSsoft	45
5.10	2-D configuration of stage 3 from KISSsoft	45
5.11	Configuration for a planet gear.	47
5.12	Configuration for a sun gear.	47
A.1	Rotor Torque for 4,6,8 and 10 m/s wind speed, from OpenFAST.	55
A.2	Rotor Torque for 12,14,16 and 18 m/s wind speed,from OpenFAST.	56
A.3	LDD for 4,6,8 and 10 m/s wind speed.	56
A.4	LDD for 12,14,16 and 18 m/s wind speed.	57
A.5	Stage 1, final configuration design.	66
A.6	Stage 2, final configuration design.	67
A.7	Stage 3, final configuration design.	67

Acronyms

BEM

Blade Element Momentum

CAPEX

Capital Expenditures

DD

Direct Drive

DLC

Design Load Case

DSL

Design Standard Requirements

FA

Fatigue Analysis

FAST

Fx Adapted for SStreaming

HAWC2

Horizontal axis Wind Turbine simulation Code 2nd generation

HS

High-Speed

IEA

International Energy Agency

IEC

International Electrochemical Commission

LDD

Load Duration Distribution

MOST

Matlab for Floating Offshore wind turbine

MS

Medium-Speed

US

Ultimate Strength

Chapter 1

Introduction

1.1 Motivation

It's the end of the IIWW, and humanity has to face significant changes in their lifestyle: modernization and intense industrialization, which is a phenomenon started after the Industrial Revolution and followed by intense urbanization, pushing people to leave the countryside to find fortune in the main cities of Europe. At the same time, the increment of welfare in the "Old Continent" and, mostly, in the developing countries of BRICS (an acronym which stands for Brazil, Russia, India, China, and South Africa), as well as better sanitary conditions with the progress in the medical field, lead to the increase of the world population, reaching up values almost around eight billion of people nowadays. Those conditions can be enclosed as the main reason behind the increment in energy consumption in Europe and any other country.

Focusing on the European Union, this growth interests three significant sectors: industry [26.1%], household [28.0%], and transport [28.4%], even though substantial percentages can also be observed for services and agriculture-forest fields [respectively 13.7% and 3.2%].

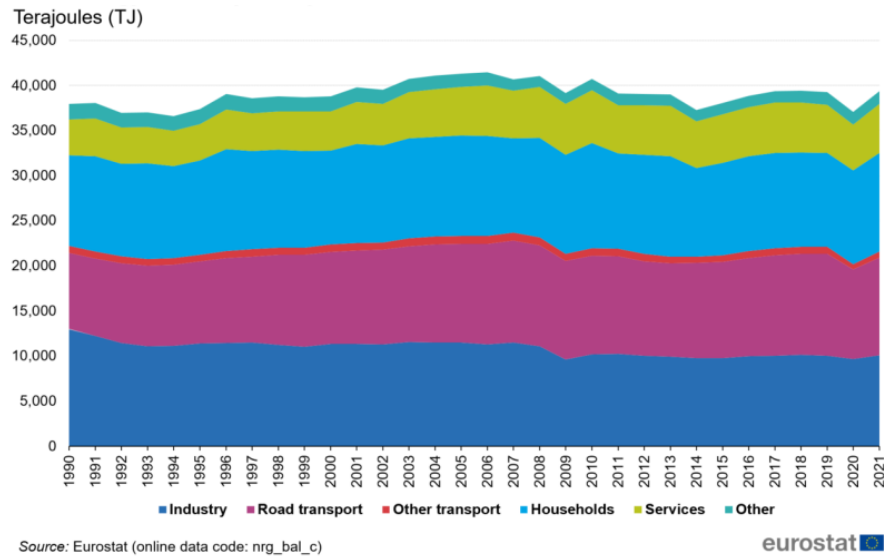


Figure 1.1: Final energy consumption by sector, EU, 1990-2021, Terajoules (TJ)

Looking closely at the graph, Fig.1.1, the trend of energy consumption in the last decades seems to be relatively stable, with a significant peak in 2007 where the final consumption reached values around 42000 TJ, two drops in 2008 and 2013 due to the economic crisis and a more considerable reduction in 2020 [final energy consumption of 37000 TJ] due to the Covid-19 pandemic which interested almost every sector but the industry, which trend remained virtually unchanged [1].

Strictly connected to energy consumption growth, new challenges must be faced by the European Community, starting with the problem of climate change and global warming. Most of the time, those two concepts need to be understood and clarified. Global warming is the long-term heating of the Earth's surface observed since the pre-industrial period due to the increment of greenhouse gases trapped in the Earth's atmosphere caused by several human activities, such as fossil fuel burning. On the other side, climate change is the long-term change in the average weather patterns that define the local and global climate, noticed since the 20th century. Climate change is the consequence of global warming[2].

Moving to the second graph reported in this chapter, Fig.1.2, Europe is a poor continent regarding energy products on the territory; thus, the necessity of imports from outside has become increasingly significant.

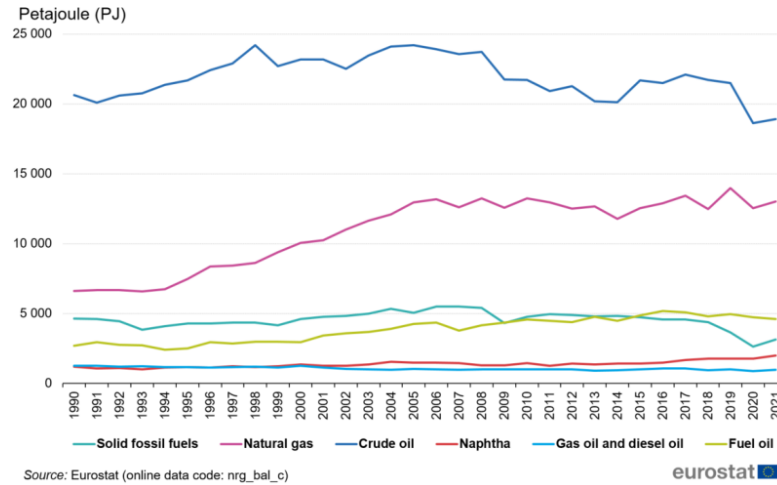


Figure 1.2: Imports of selected energy products, EU, 1990-2021 Petajoule (PJ).

Natural gas, the second largest imported product after crude oil, is in constant demand. Russia is the country which, until 2022, represented the major importer with a percentage up to 29 %, followed by the USA and Norway. Unfortunately, the Russian war in Ukraine made the importation stop, bringing up the issue of dependency rate, a hot topic discussed all year. This term represents the extent to which an economy relies upon imports to meet its energy needs, and the share of net imports in gross inland energy consumption gives it. The high value of this rate shows once again how fragile is the energy production in Europe [1]. Hence, the need to find new ways of producing energy from renewable sources while improving the current systems. This thesis will focus on a specific renewable source: the wind flowing over the sea, thus wind energy and offshore wind turbines.

1.2 Objective

The main objective of this thesis is to design a gearbox that could be implemented for a 22 MW offshore wind turbine. By the completion of this thesis, a literature review on wind turbine aerodynamics and the IEC standards for an offshore wind turbine should be comprised. A global analysis gathers all wind data, torque, and wind speed, which are fundamental for the gearbox modeling according to the local analysis and IEC standards. The design is carried out using OpenFAST and KISSsoft, and the modeling of the main components of the gearbox, gears, and bearings is performed for both the Fatigue and Ultimate Load analysis, whose values are obtained from OpenFAST during the global analysis previously performed.

1.3 History and developement

Wind energy has a millennial history from the birth of human civilization following its development through time. The first form of a wind system is the windmill, born apparently in ancient Babylon around 2000 BC, spreading through Europe many centuries later, in 1100 AD, in France, where the structure was slightly different because the motion wasn't anymore vertical but on the horizontal axis [3]. Nevertheless, those applications were mechanical and meant just for farming. You have to wait until late 1800 when the first generator was invented and introduced in the wind system, making it able to produce electricity [3] and in 1887 the first wind turbine was built in the USA with a power production of 12 KW. Since the last century, wind energy has become one of the symbols of a clean and efficient system for electricity production intertwining with aeronautical studies, and in 1980, New Hampshire, USA, it was built the first wind farm with 20 wind turbines. Unfortunately, the fate of this wind farm was not in its favor.



Figure 1.3: Wind turbines at sea. Author: CGP Grey. License: Creative Commons, Attribution 2.0 Generic.

Better was the case of Denmark, which was able to build in 1991 the first offshore wind farm with 11 turbines and a total power production of 450 KW [4]. It's with the new millennium that an increment in productivity is possible to see for those systems. Starting in 2005, when an extensive formation alone produced 90 MW, up to 2006 when the biggest offshore wind farm in the North Sea began to be constructed with more than 300 wind turbines.

What next? Many projects for possible future developments have been discussed to have more efficient and productive plants. In China, close to the city of Chaozhou, the government is planning a wind farm that would dwarf all the Norwegian power

plants combined, or moving back to Europe, the UK government's goal is to build a power plant of 50 GW wind capacity by 2030 [5]. Something less ambitious but similar is thought by EQUINOR company with the target to reach a net capacity of 12-16 GW by the same year[6]. Higher power production is not the only parameter companies seek; sustainability and environmental attention are also considered. New researchers are looking for offshore floating wind turbines as a good connection point since they do not need to be grounded in the seabed, and therefore, they can be seated further from the shore at a water depth greater than 60m, where the wind is stronger, and the installation occurs with way less noise and disruption to marine fauna. Unfortunately, the anchors and mooring lines still need to be monitored for their impacts on the life of the seafloor, plus the CAPEX results to be greater than the regular wind turbines [7]. Through larger systems (in terms of power), better design, and streamlined operation, it is predicted that offshore wind turbines will be commercialized without any support scheme in the next few years.

1.4 Structure of the thesis

The thesis is divided into six chapters strictly connected to each other. In Chapter 1, the theme of the thesis is presented with a brief description of its primary motivation and its objective. Chapter 2 is a theoretical chapter explaining the theory behind the turbine design, fundamental for the following two chapters (3 and 4), where the global analysis and the local analysis are performed with the auxiliary of two peculiar software, OpenFAST and KISSsoft. The results are presented in Chapter 5, followed by the discussion and description of the main outcomes. The conclusions are drafted in the last chapter, Chapter 6, alongside a few recommendations for further work.

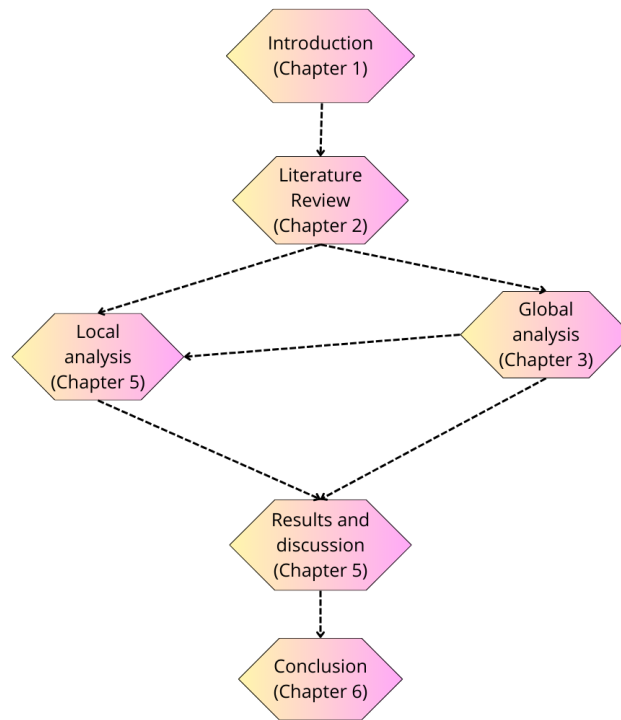


Figure 1.4: Flow chart of the structure of the thesis.

Chapter 2

Literature Review

This section of the thesis presents the state-of-the-art of a generical wind turbine, followed by a literature review regarding wind turbine aerodynamics and IEC Standards. A brief overview is also offered for the peculiar software that can be used for the global and local analysis of the turbine.

2.1 State of art of wind turbine

A wind turbine is an electro-mechanical device able to produce renewable energy from wind by converting its high kinetic energy into electricity.

2.1.1 Classification

Many different types of wind turbines could be distinguished according to:

- Rotational axis
- Production power
- Location

Wind turbines may have a horizontal axis (HAWT) or a vertical axis (VAWT).

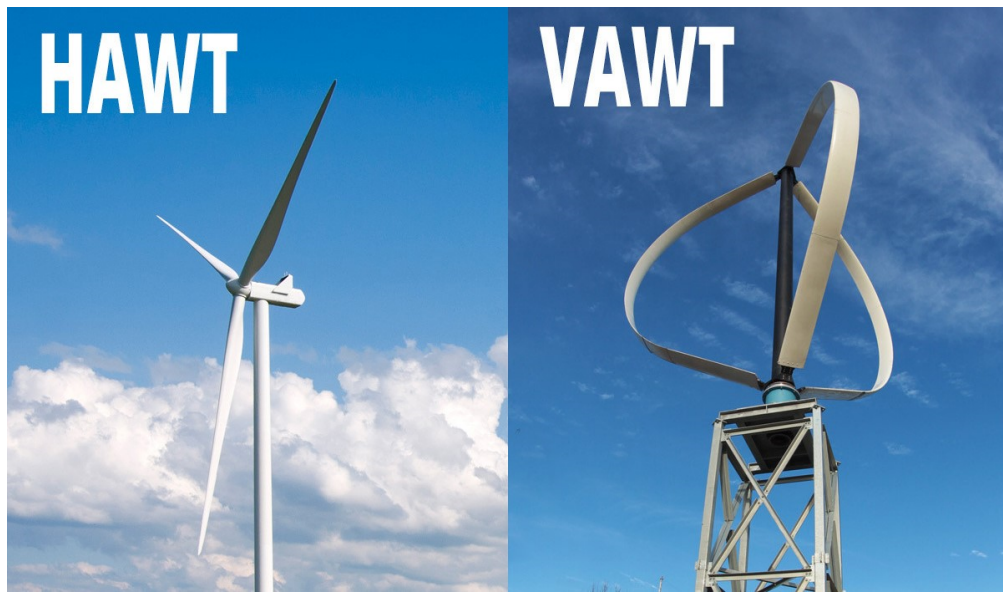


Figure 2.1: Vertical and Horizontal axis wind turbine, arborwind.com

HAWT systems are widely used for many applications and can be further classified by the number of blades, varying from two to three. Two-blade wind turbines are less preferred because, even though they are cheaper, the necessity of a higher rotational speed leads to low efficiencies. Plus another drawback of this kind of technology is the flickering. Therefore, it is prone to use three-blade wind turbines to achieve the desired power for considerable demands. On the other hand, VAWT can differ according to the operational principle based on the exploitation of lift and drag. Nonetheless, these systems are likely used for small power production.

Focusing on the power, it is further possible to identify three other classes of wind turbines according to the power delivered to the grid. A wind turbine is called "small" when it can produce less than 100 KW, "medium" for power production between 100 KW and 1 MW, and "big" when it comes to more than 1 MW produced power. This last category is the most diffused in the market but is still under study for ulterior improvement.

Lastly, the location of the wind turbine is fundamental to performing the case studies and analysis correctly; thus, a wind turbine can be onshore if built on the mainland or offshore if in the sea/ocean. According to the type of the tower's foundations, offshore wind turbines can be classified as "fixed-bottom" or "floating"[8].

2.1.2 Wind turbine main components

As is possible to see from Fig. 2.2 wind turbines are characterized by three main parts: blade-rotor, nacelle, and tower-foundation.

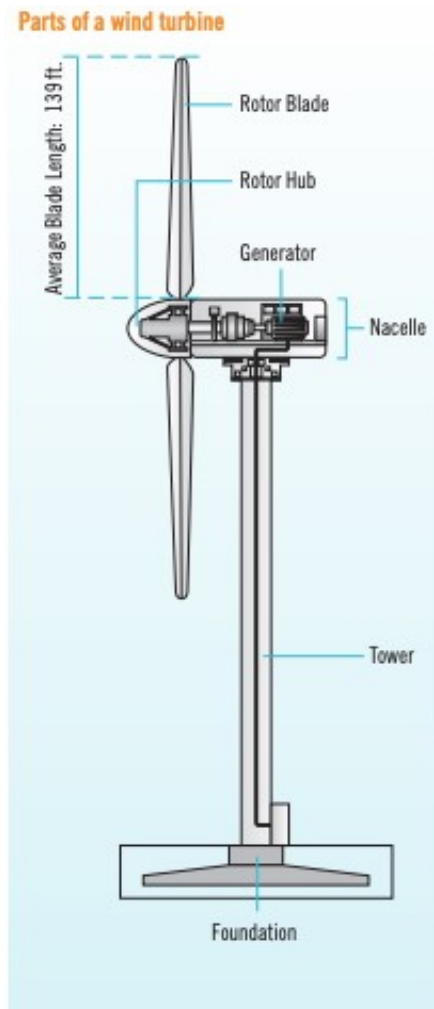


Figure 2.2: Wind turbine structure, sustainable.solutions.duke-energy.com

A wind turbine's rotor is the combination of blades and hub, and it's the place where the wind's kinetic energy is transformed into mechanical rotation of the shaft. At the same time, the blades are light and resistant, built with composite materials strengthened by glass and carbon fibers. The next component connected to the rotor is the nacelle: a simple housing structure containing all the components of the drivetrain (whose configuration is presented in section 2.1.3), an anemometer, a control-protection system, and a braking system. The brakes should be able to

slow down the rotor during adverse weather conditions and can be aerodynamic or mechanical. The design of a wind turbine is always such that the nacelle is accessible for maintenance or repairs. The nacelle is wholly supported by the tower, whose dimensions could reach a hundred meters to handle the wind loads. There are many configurations, from tubular steel towers to lattice towers, with several advantages and drawbacks. The tower is fixed to the bottom by well-designed foundations, which can be slightly different for onshore or offshore turbines[8].

2.1.3 The drivetrain

The wind turbine's drivetrain aims to convert low-speed and high-torque rotation from the rotor into electricity. It contributes to the total energy cost produced by the wind turbine since it includes some of the most costly components with a high level of technology risk.

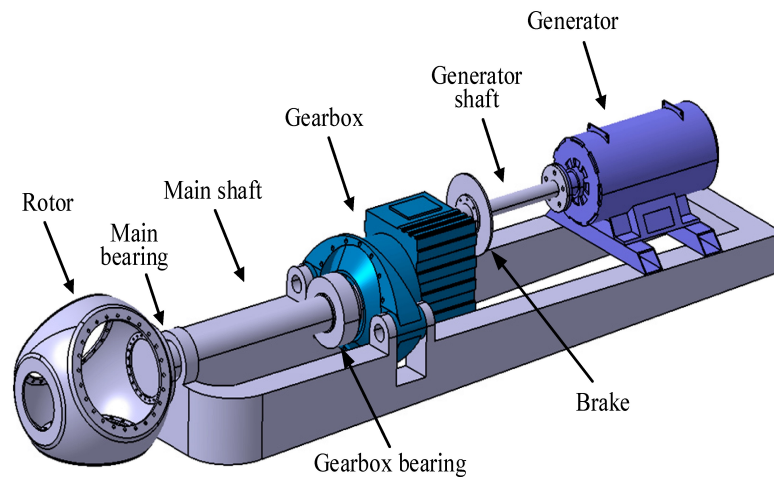


Figure 2.3: Drivetrain structure, Qian, P., Ma, X., and Zhang, D. Estimating Health Condition of the Wind Turbine Drivetrain System

The main components of the drivetrain are shown in Fig.2.3

1. main bearing
2. main shaft
3. gearbox bearing
4. gearbox
5. high-speed shaft or generator shaft

6. generator

7. brake

The rotor hub is connected to the nacelle by the low-speed shaft, also known as the main shaft, which is supported by the mainframe through one of the two main bearings, which also aims to minimize friction between the moving parts of the turbine. The main shaft transmits the rotation to the gearbox, aiming to increase the speed, reaching values up to 1800 rpm. Depending on the turbine power, the gearbox configuration can include two or three stages, and a choice between a planetary or parallel gear topology can be made. The necessity to increase the speed is linked to the requirements of the generator to economically produce electrical energy. Despite having diverse configurations of generators, such as AC synchronous or asynchronous generators, the working principle is always based on electromagnetic induction. It may also use power electronics to allow variable-speed operations[8].

2.2 Wind turbine Aerodynamic

Aerodynamics is one of the primary topics in wind turbine research because the design of a flow control mechanism lays the foundation for an efficient power output.

2.2.1 The wind

The global wind system is dominated by large-scale high and low-pressure systems casually distributed worldwide. Plus, being in a rotational system means the presence of a fictive force called the Coriolis force.

Let's consider a generical point P in an absolute reference system. Thus, its acceleration would be:

$$a_{abs}^{\vec{}} = a_{rel}^{\vec{}} + 2\vec{\omega} \times v_{rel}^{\vec{}} + \vec{a}_0 + \vec{\omega} \times \vec{r} + \vec{\omega} \times \vec{\omega} \times \vec{r} \quad (2.1)$$

where:

- the first two terms of the equation 2.1 represent the acceleration of P in the relative system
- the last three are the acceleration of P, if P is at rest in the relative system

Now, assuming that the origin 0 of the relative system is located in the Earth's center of mass, the Earth's velocity would be constant, thus \vec{a}_0 and $\vec{\omega}$ are null. Furthermore, $\vec{\omega} \times \vec{\omega} \times \vec{r}$ has the same direction of the gravity acceleration but with

a smaller module, and that makes it possible to neglect it. Then, the final equation would be:

$$a_{abs}^{\vec{}} = a_{rel}^{\vec{}} + 2\vec{\omega} \times v_{rel}^{\vec{}} \quad (2.2)$$

The Coriolis acceleration $2\vec{\omega} \times v_{rel}^{\vec{}}$ in the northern hemisphere is directed 90° to the right of $a_{rel}^{\vec{}}$ while in the southern hemisphere is 90° to the left due to the opposite spin. The magnitude of the Coriolis acceleration

$$|a_{cor}^{\vec{}}| = |2\vec{\omega} \times v_{rel}^{\vec{}}| \quad (2.3)$$

is maximum at the poles and zero at the equator. Generally speaking, the values of the Coriolis acceleration are pretty much small but still significant when it comes to transporting large masses, such as air and water.

Now, let's consider high-pressure (H) and low-pressure (L) areas close to each other: a driving force from H to L exists, causing acceleration and nearby velocity from H to L. This velocity creates the Coriolis force, which will try to change its direction until a balance between the pressure and Coriolis forces is reached. This condition is possible to observe at high altitudes (1 Km more or less) where the friction can be negligible, and it's called geostrophic flow. This flow is impossible for wind turbines since their height is a maximum of a hundred meters, and the definition of wind with a stochastic behavior should be considered. Plus, the wind is a 3-D phenomenon; therefore, the total wind velocity equation is:

$$\vec{U}(x, y, z) = [\vec{U}(z) + u(x, y, z)]\vec{i} + v(x, y, z)\vec{j} + \omega(x, y, z)\vec{k} \quad (2.4)$$

where u, v , and z are the components of the wind gust vector \vec{U}' , while $\vec{U}(z)$ is the mean wind component. The mean velocity profile for the wind over the ocean is given by:

$$\vec{U}(z) = 2.5U_{10}\sqrt{x} \ln(z/z_0) \quad (2.5)$$

where U_{10} is the velocity at 10 m above the ocean, usually obtained from the Weibull distribution, x is the sea drag surface, and z_0 is the roughness due to waves. The wind gust over the open ocean can be measured similarly as the wind over the land, thus by the Harris and Davenport analysis, but if the installation of the wind turbines is closer to the shore, then the Ochi and Shin analysis results to be more effective: the spectral formulation obtained is presented as an average of several wind gust spectra obtained from measurements over waves [9].

2.2.2 Aerodynamic forces: lift and drag

The interaction between the airflow and the stationary and moving parts of wind turbines leads to the formation of the aerodynamic forces of lift and drag, which

the wind turbines exploit to produce electricity. Consider an aerofoil-shaped body, such as the rotor blade of the wind turbine; due to the shape, streamlines are forced to curve around the geometry, and since fluid particles are changing direction, a centripetal force is acting. The cause of the existence of this force must be sought in the presence of a pressure gradient between the upper and lower parts of the body:

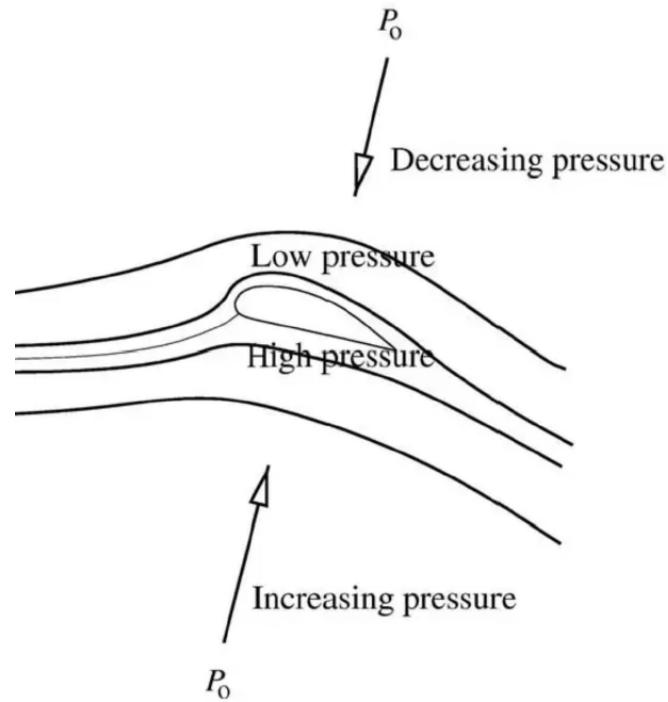


Figure 2.4: Pressure gradient between upper and bottom part of a body

$$\nabla P = \frac{\partial p}{\partial R} = \rho \frac{V^2}{R} \quad (2.6)$$

where V is the wind speed and R is the curvature of the streamline. In order to be generated, lift force requires two conditions:

- motion $\rightarrow v_{object} \neq v_{wind} \neq 0$
- fluid

It works through the center of pressure of the object and it is directed perpendicular to the wind speed.

$$F_l = \frac{1}{2} \rho V^2 c C_l \quad (2.7)$$

Also, drag force is applied on the center of pressure of the body but parallel to the wind speed and opposite to the thrust.

$$F_d = \frac{1}{2}\rho V^2 AC_d \quad (2.8)$$

It is generated by the difference between wind and body speed and can be classified into two categories:

1. Parasitic drag due to surface friction
2. Induced drag due to the generation of lift

Drag and Lift coefficients, respectively C_d and C_l , are fundamental to computing the output power from the wind turbine.

Moreover, the body is subjected to a moment, which is applied to a point located on the chord line at $\frac{C}{4}$ from the leading edge and defined as positive when it tends to turn the aerofoil clockwise (nose up).

$$M = \frac{1}{2}\rho V^2 c^2 \quad (2.9)$$

Note that all the coefficients are a function of:

- α angle of attack, or better the angle between the chord line and the wind speed vector
- Reynolds number
- Mach number, even though it is not contemplated for wind turbine [10]

2.2.3 Stall condition

Air is a fluid with low viscosity, sometimes negligible, but when it comes to the wind turbine's analysis, it is the main reason behind the formation of a boundary layer on the blade's surface.

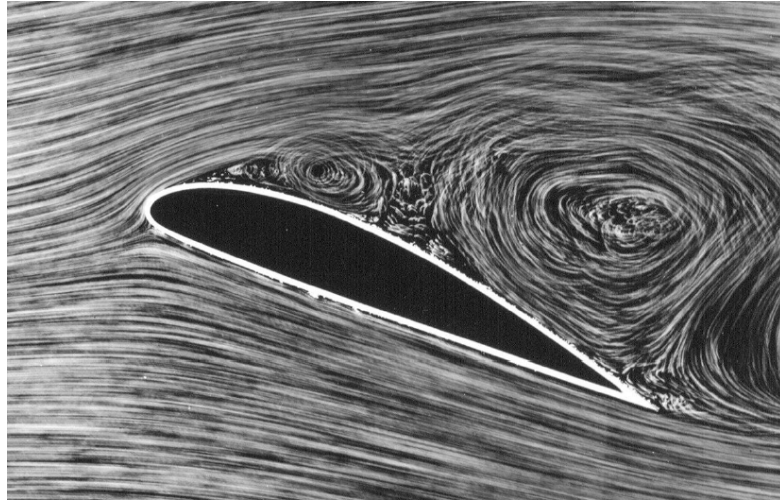


Figure 2.5: Stall condition

Lift coefficient C_l increases linearly with the angle of attack α until it reaches a maximum value. Then, if α still grows, C_l will decrease in a geometrically dependent manner while C_d becomes more critical. Plus, if the angle of attack of the blade is higher than the steady state stall angle of attack due to turbulence or gust or yaw misalignment, the boundary layer separates from the upper part of the aerofoil, starting at the trailing edge and increases slowly with the angle of attack. This condition causes a reversal flow that stops the fluid, and viscous forces make it rotate, forming vortices. The dynamic stall is the primary source of unsteady loads and reduces the performance and fatigue life of the wind turbine. Stall can be worsened if the separation starts at the leading edge because, in this case, the entire boundary layer may be separated simultaneously, causing a dramatic loss of lift[10].

2.3 BEM method for wind turbine

The Blade Element Momentum model is a widely used tool to design many wind turbine components and calculate steady loads, thrust, and power for different wind speeds, pitch angles, and rotational speeds. It can model the aerodynamic interactions between a turbine and a fluid flow through algebraic relations.

The model is based on several hypotheses that make analytical resolution easier:

1. 1-D model that applies the conservation of the momentum to N annular domains of height dr .
2. Unidimensional flow, incompressible and constant in time.

3. No radial inter-dependence, thus what happens at one element can not be felt by others.
4. Infinite number of blades.

Now, consider the conservation of momentum equation:

$$\frac{\partial}{\partial t} \int \int \int_{cv} \rho u(x, y, z) dx dy dz + \int \int_{cs}^0 \rho u(x, y, z) V dA = F_{ext} + F_{pres} \quad (2.10)$$

For stationary flow and for an applied torque on the edges of the annular control volume equal to zero, the moment of momentum is:

$$M = \int \int_{cs}^0 r \times V \rho V dA \quad (2.11)$$

which be also derived from the mechanical power removed from the disc on the control volume:

$$dP = \omega dM \quad (2.12)$$

thus, for a control volume of area $2\pi r dr$:

$$dM = r m C_\theta = 2r^2 \pi \rho u C_\theta dr \quad (2.13)$$

where C_θ is the rotational velocity in the wake and u the axial velocity of wind.

On the other hand, the thrust on the rotor has been found by applying Bernoulli's equation before and after the rotor and introducing at the same time the conservation of the axial momentum and mass:

$$\Delta P = \frac{1}{2} \rho (V_0^2 - u_1^2) \quad (2.14)$$

$$dT = (V_0 - u_1) d\dot{m} = 2r\pi\rho u (V_0 - u_1) dr \quad (2.15)$$

From 1-D Momentum Theory, the axial induction factor ' a ' is defined and permits to correlates the velocities u_1 , axial velocity in the wake, and V_0 :

$$u_1 = (1 - 2a)V_0 \quad (2.16)$$

Similar considerations can be done also for the moment equation, thus the final form for equations 2.13 and 2.15 is:

$$dM = 4\pi r^3 \rho V_0 \omega (1 - a) a' dr \quad (2.17)$$

$$dT = 4\pi r \rho V_0^2 a (1 - a) dr \quad (2.18)$$

Now, let's define Θ as the local pitch angle, α as the local angle on attack and Φ as the local flow angle so that

$$\alpha = \Phi - \Theta \quad (2.19)$$

$$\tan\Phi = \frac{(1-a)V_0}{(1+a')\omega r} \quad (2.20)$$

and consider the aerodynamic forces of lift and drag, supposing to know both coefficients.

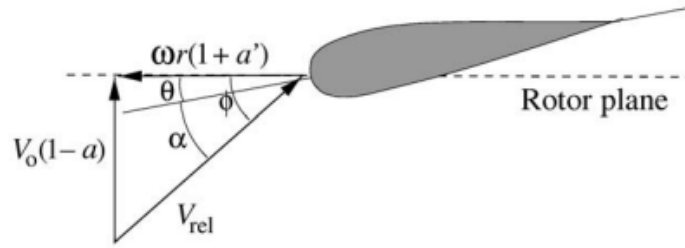


Figure 2.6: Velocities at the rotor plane

Since the interest is only for their projection on normal and tangential rotor plane, then the module of the total forces per length in these two directions would be:

$$p_n = F_l \cos(\Phi) + F_d \sin(\Phi) \quad (2.21)$$

and

$$p_t = F_l \sin(\Phi) - F_d \cos(\Phi) \quad (2.22)$$

and they can be further normalized with respect to $\frac{1}{2}\rho V^2 c$ yielding:

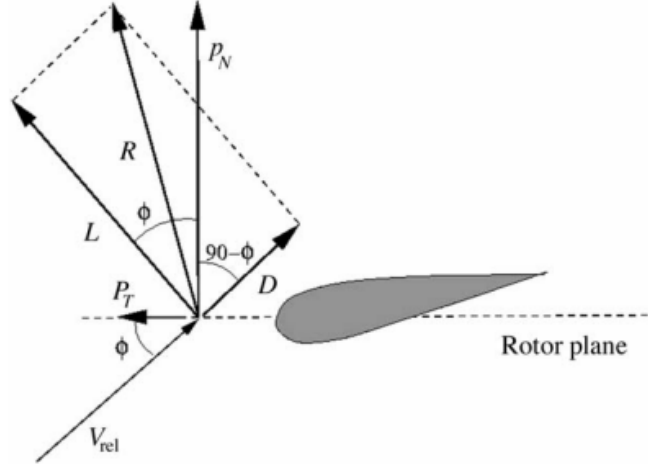


Figure 2.7: Local loads on the blade

$$C_n = C_l \cos(\Phi) + C_d \sin(\Phi) \quad (2.23)$$

$$C_t = C_l \sin(\Phi) - C_d \cos(\Phi) \quad (2.24)$$

Then, it is possible to define another important parameter, called solidity σ , as the fraction of the annular area in the control volume covered by the blades:

$$\sigma(r) = \frac{c(r)B}{2\pi r} \quad (2.25)$$

where $c(r)$ is the local chord, B the number of blades and r the radial position of the control volume.

Thus, it is now possible to write the final equations for the thrust and the moment:

$$dt = Bp_n dr \quad (2.26)$$

$$dM = rBp_t dr \quad (2.27)$$

The equations 2.26 and 2.27 can be further developed by considering the correlations between V_0 , V , and ω and from Figure 2.6 it is readily seen from the geometry that:

$$V \sin(\Phi) = V_0(1 - a) \quad (2.28)$$

$$V \cos(\Phi) = \omega r(1 + a') \quad (2.29)$$

therefore:

$$dT = \frac{1}{2}\rho B \frac{V_0^2(1-a)^2}{\sin^2(\Phi)} cC_n dr \quad (2.30)$$

$$dM = \frac{1}{2}\rho B \frac{V_0(1-a)\omega r(1+a')}{\sin(\Phi)\cos(\Phi)} cC_t r dr \quad (2.31)$$

If the equations 2.30 and 2.31 with respectively the equations 2.18 and 2.17, what is obtained is an analytical expression for the coefficients a and a' :

$$a = \frac{1}{\frac{4\sin^2(\Phi)}{\sigma C_n} + 1} \quad (2.32)$$

$$a' = \frac{1}{\frac{4\sin(\Phi)\cos(\Phi)}{\sigma C_t} - 1} \quad (2.33)$$

Once the BEM method has been derived, the power curve could be computed as the shaft power as a function of wind speed. Note that the production must be corrected due to losses in the generator and gearbox, whose combined efficiency is 0.9. [10]

2.3.1 Prantl's tip loss factor

Prantl's tip loss factor is added as a correction for the infinite number of blades hypothesis. When it comes to a rotor with a finite number of blades, the vortex system in the wake is dissimilar compared to the case of a rotor with an infinite number of blades, thus the introduction of a correction factor is required:

$$F = \frac{2}{\pi} \cos^{-1}(e^{-f}) \quad (2.34)$$

where

$$f = \frac{B}{2} \frac{R-r}{r \sin(\Phi)} \quad (2.35)$$

Therefore, the moment and thrust equations:

$$dT = 4\pi r \rho V_0^2 a(1-a)F dr \quad (2.36)$$

$$dM = 4\pi r^3 \rho V_0 \omega (1-a)a'F dr \quad (2.37)$$

2.3.2 Glauert correction

Glauert correction is applied when the numerical value of a becomes larger than 0.4, and it is only used for the thrust coefficient:

$$C_t = 4a(1 - \frac{1}{4}(5 - 3a)a)F \quad (2.38)$$

Note that when a is larger than 0.2-0.4, then the simple momentum theory breaks down.[10]

2.3.3 Unsteady BEM model

Because of the unsteadiness of the wind, induced by some factors like atmospheric turbulence, the aeroelastic behavior of the wind turbine should be computed more realistically by introducing the unsteady BEM model. In a few words, the unsteady BEM model is about a more or less complex model that requires the set of a fixed coordinate system of any section along the blade, and it has to deal with the wind changing in both time and space.[10]

2.4 DSL - Design Standard Requirements

The Design Standard Requirements are simple guidelines to set the design requirements for wind turbines to build them adequately engineered against damage. Many types of DSL are called by different names and developed in sundry countries. For this project, the standards looked at are the ones defined by the IEC (International Electrochemical Commission), and more specifically:

- IEC 61400-1 -> design requirements to ensure the structural integrity of a wind turbine
- IEC 61400-3 -> design requirements for offshore wind turbines

2.4.1 IEC 61400-1

Standard IEC 61400-1 [11] specifies the basic design requirements to secure the structural integrity of the turbines and divides them into several classes according to the wind speed (classes I, II, and III) or the turbulence parameter (classes A^+ , A, B, and C).

The table below shows the basic parameters associated with each wind turbine class.

WIND TURBINE CLASS		I	II	III	S
V_{ave}	(m/s)	10	8.5	7.4	Values Specified by the designer
V_{ref}	(m/s)	50	42.5	37.5	
	Tropical (m/s)	57	57	57	
A+	I_{ref} (-)	0.18			
A	I_{ref} (-)	0.16			
B	I_{ref} (-)	0.14			
C	I_{ref} (-)	0.12			

Table 2.1: Basic parameters for wind turbine classes.

Along with the classes reported before, there are also other classifications of wind turbines based on extreme external conditions, such as tropical cyclone (class T) or frigid weather (class CC).

This standard is also essential for defining wind conditions, structural analysis, and load calculation; above all, the ultimate limit analysis section quotes the various values for the partial safety factor according to the component class for fatigue and static failure. Plus, a whole vision of the mechanical part is given, even though for the definition of an offshore wind turbine drivetrain, the specification that has to be looked at is the standard IEC 61400-4.

2.4.2 IEC 61400-3

Standard IEC 61400-3 [12] sets the design requirements for a fixed-bottom offshore wind turbine to guarantee engineering integrity and the assessment of external conditions.

The definition of the wind condition is already described in Standard 61400-1, but further components must be added:

- extreme 10 minutes average wind speed at hub height $V_{1,hub}$ with a return period of 1 year
- wind speed standard deviation $\hat{\sigma}$ from the ambient turbulence.

All the parameters should be available as a function of wind direction and given as a 10-minute average. However, if there is no data, the surface roughness parameter z_0 can be used to estimate them.

Furthermore, a section about the design situations and load cases is present to verify the offshore wind turbine's structural integrity. Load cases shall be determined from a combination of operational modes or other design conditions, as shown in the following table.

DESIGN CONDITION	DLC	TYPE of ANALYSIS	PARTIAL SAFETY FACTOR
1) Power production	1.1	U	N (1.25)
	1.2	F	*
2) Power production plus occurrence of fault	2.2	U	A

Table 2.2: Example of Design Load Cases defined in EIC 61400-3.

where F stands for fatigue load, while U is for analysis of ultimate loads, which can be further divided into normal loads N , that occur frequently or abnormal loads A .

2.5 Design tools for an offshore wind turbine

During the process of designing a gearbox of an offshore wind turbine, many peculiar software can be used. For this specific case, OpenFAST and KISSsoft are the ones selected respectively for the global and local analyses.

OpenFAST is an open-source wind turbine simulation tool that was established with the FAST v8 code as its starting point and it has been processed recently to compute different analyses of a range of onshore and offshore wind turbine configurations, relying on developing a graphical representation that shows logical links between project functions. It joins aerodynamic and hydrodynamics models with structural dynamic models throughout modular interfaces and couplers. This software was developed by Jason Jonkman, Ph.D., Mike Sprague, Ph.D., and colleagues of NREL [13]. The implementation of a 22 MW wind turbine project in FAST is shown in the last section of Chapter 3. KISSSoft is a modular calculation program able to size, analyze, and optimize machine elements and gearboxes. At the same time, it provides effective analysis tools for gear manufacturing and inspection. This software is implemented in the local analysis study for gears and bearings of the gearbox, Chapter 4.

In addition to OpenFAST and KISSsoft, many other design tools and software can be used for the gearbox definition, such as MOST, a fast simulation model for optimization of floating offshore wind turbines in Simscape Multibody [14], or HAWC2 (Horizontal Axis Wind turbine simulation Code 2nd generation), which is an aeroelastic code able to calculate wind turbine response in time domain. The software is used for design and verification purposes [15].

Chapter 3

Global Analysis for the 22MW Wind Turbine

3.1 Location definition

To select the proper location for the 22 MW wind turbine, different features are taken into account. First, the Surf-forecast website is consulted to understand the wave and wind characteristics throughout the day. This website is highly detailed and reliable, but unfortunately, it gives back just the wind and ocean conditions of the same day of the check, plus the ones of the past and the following two days. Thus, to have a better overview, the website is monitored for at least three days in a row. The parameters gathered to define the correct site are the intensity and direction of the wind, the height of the waves, and the surface temperature. Plus, the Norwegian normative and legislation are checked to identify the hypothetical presence of marine protected areas close to the coasts and the regulations and requirements for the marine devices installation. Finally, to estimate the distance from the shore, the trend of the seabed and the total height of the turbine tower are considered while considering the local laws to avoid noise pollution and disturbance of the ecosystem.

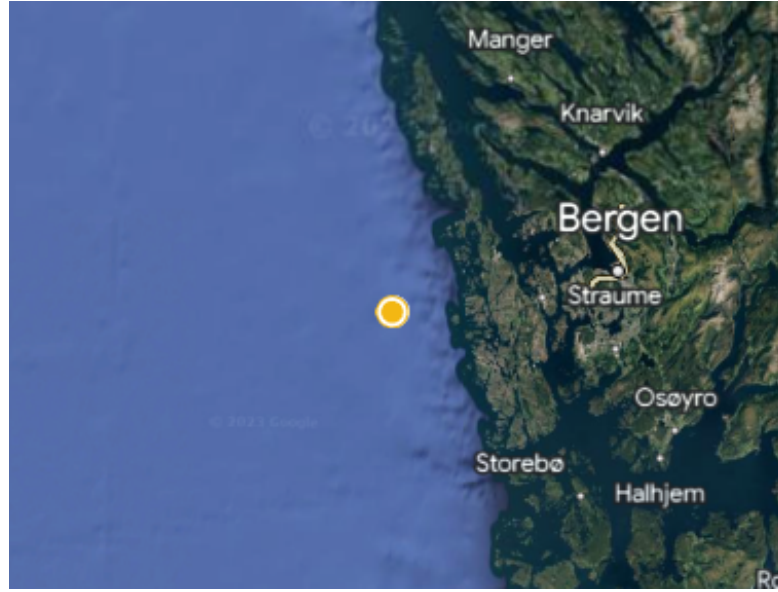


Figure 3.1: 22MW Wind Turbine Location from Google Earth

Among four initial suggestions (Hitra Island, Ålesund, Stavanger, and Bergen), the chosen location is 9 Km from Bergen's coast Fig.3.1, far from marine protected areas, and whose features are shown in the following table:

COORDINATES	60° 21' 21.3"	N
	4° 50' 41.2"	E
DISTANCE FROM COAST	11.03	m
WATER DEPTH	190	m

Table 3.1: Characteristic of the location where the turbine is supposed to be installed.

In the same area, one of the most important sites in Norway where offshore wind turbines are tested is also located.

After choosing the location, to check if the selection is corrected, the values of the wind gust, wave height, and period have been gathered from Matlab. The first step is to open the file ERAFIVEData-extraction.m, where the link for a wind website is in line 1. On the website, the values of the required parameter are:

- 100m u-component of wind (u_{100})
- 100m v-component of wind (v_{100})
- Significant height of combined wind waves and swell (H_s)

- Peak wave period (T_p)
- Mean wave direction (D_{irm})

and they are obtained for two years by selecting for the wanted location all the months, days, and hours. Those values are saved in a file directly downloaded in the same folder of ERAFIVEdata. Then, after changing the name of the file at lines 38 and 39, another Matlab file, simplify-triplet.mlx, is opened, and here, wind gust and wave height and period are represented by detailed plots, which are possible to observe in the first section of Chapter 5. Those values are then inserted in RunTurbsim.m.

Finally, the Weibull Distribution for the wind over the ocean is obtained from the wind gust plot.

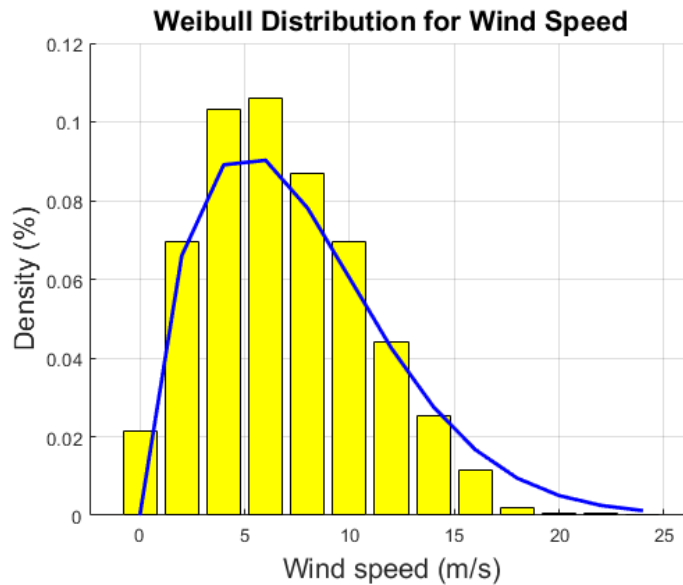


Figure 3.2: Weibull Wind speed distribution for the chosen location.

All the Matlab scripts can be consulted in Appendix A.

3.2 22 MW wind turbine

The design of the drivetrain of the 22 MW offshore wind turbine is based on the reference given by IEA Task 37. The goal of IEA 37 is to improve both the practice and the application of system engineering to wind energy research design, development, and operation, followed by three targets of impact (Research-industry collaboration, education, and wind energy system performance-cost). Currently,

the project is stuck in the second phase since 2020. The model given for the 22 MW is gathered from the Github repository, and it is just a "pre-release": it can still undergo frequent and significant changes by the IEA Task 37 partners; thus, the current values obtained are just hypothetical. Plus, this model is only suitable for a three-blade, fixed-bottom offshore wind turbine. [16]

3.3 Design Load Cases and Global Analysis for the 22 MW turbine

The Design Standard Requirement document IEC 61400-3 [12] presents a subsection regarding Design situations and Load cases, which are fundamental to running the FAST model of the turbine correctly in different conditions so that realistic comparisons can be made. In the following table, the chosen load case is listed with its features:

DESIGN CONDITION	Power production
DLC	1.1
Wind	NTM $V_{in} < V_{hub} < V_{out}$
Waves	NSS
Wind and waves directionality	COD ,UNI
Type of analysis	U
Partial safety factor	N (1.25)

Table 3.2: DLC for the 22 MW wind turbine main features.

The load cases shall be determined from the combination of operational modes or other design situations, and all relevant load cases with a reasonable probability of occurrence shall be considered, together with the behavior of the control system. For this case study, the wind conditions are the center point of focus, while waves are not considered since the design is only made for the gearbox, which is solely affected by the wind behavior.

Once the chosen load case is defined, it is inserted in TurbsimInputFile.txt, where other parameters such as hub height and grid height and width are also changed. The simulation time T is set at 700 seconds since, according to IEC standards, the first 100 seconds represent the transient time to get the response of the turbine in order to obtain steady and accurate results, while the last 600 seconds (10-min) is the output time. The ΔT is 0.01 seconds. The IEC turbulence characteristic for the 22 MW wind turbine is class B. This selection is referred to as medium turbulence, which is more frequent for offshore turbines than onshore ones,

where turbulence is much stronger. Also, 10 and 15 MW offshore wind turbines use the same turbulence class (B).

The model is then run for wind speed from 4 up to $24 \frac{m}{s}$ with an interval of 2, and the final results are obtained (see Chapter 5 for further details).

Since the turbine is working with variable loads and wind speed, the Load Duration Distribution (LDD) analysis is performed to be able to check the fatigue life and to design the main components of the gearbox (mainly the bearings) [17]. This method is based on stress bins obtained from the input torque time series from 100 to 700 seconds. It is essential to choose the correct number of bins because it can influence the calculated fatigue damage. From the upper level of each torque bin, the stress bins are finally derived as shown in Fig. 3.3:

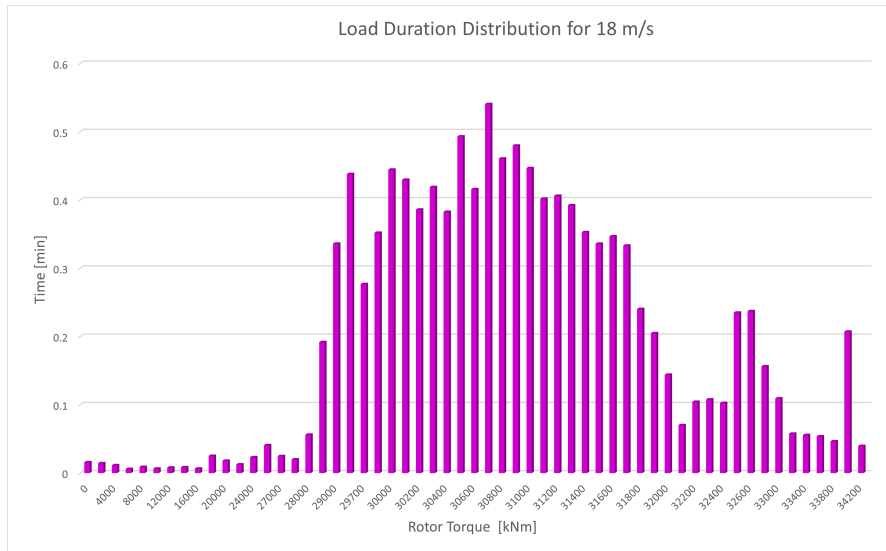


Figure 3.3: LDD for the the $18 \frac{m}{s}$ wind speed.

The gearbox design occurs in KISSsoft, a software that requires the LDD analysis to happen through all the wind speeds and with bins that have the same width. The process to obtain the data needed by KISSsoft is performed in Matlab, which script can be found in Appendix A.2.

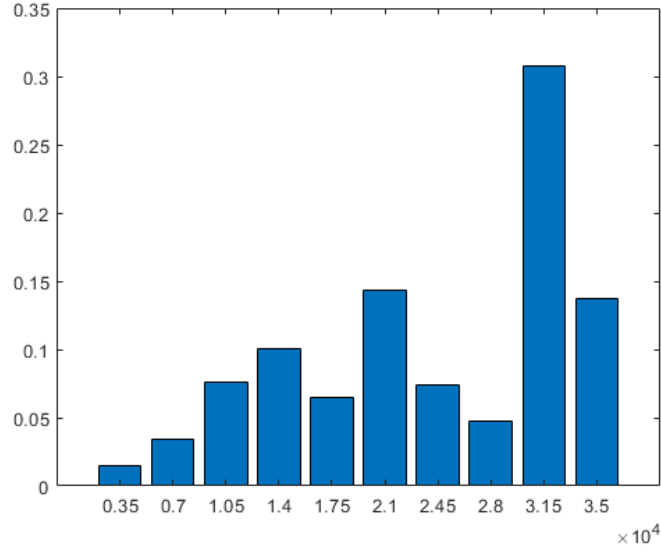


Figure 3.4: LDD for the whole wind speed range.

Finally, before starting with the design itself, the ultimate loads, also called design load F_d , must be derived. As written in IEC 61400-1[11], the first step to perform is the definition of the characteristic load F_k . Within the three methods proposed in the standard, the one chosen is based on the definition of the largest among the 99th percentile values of the 10 min extremes determined for each wind speed in the given range, multiplied by 1,2. OpenFAST has been run 15 times per wind speed with different RandSeed numbers and the rotor torque values gathered. Then, for each run of the same speed, the maximum value is chosen until a series of 15 numbers is obtained. The final step is to fit the extreme value distribution on the series and extrapolate the value which the corresponding percentile is 0.99. The process is performed in Matlab using the function `fitdist(A,'gev')` for the distribution and `cdf(pd,A)` for the percentile [18]. After the characteristic load has been defined, the ultimate load is now calculated as the product between the characteristic load and the partial safety factor γ_k , equal to 1.25 since the whole study is carried basin on the DLC 1.1.

$$F_d = \gamma_k F_k \quad (3.1)$$

The whole process is done for each wind speed, but to correctly design the gearbox, only the highest value is used, which is the ultimate load for $18 \frac{m}{s}$ wind speed.

Chapter 4

Local Analysis for the 22MW Wind Turbine

In this section of the thesis, the local analysis performed over the Gearbox of the 22 MW offshore wind turbine is described. Starting from the results obtained from the global analysis (see Chapter 5), the first step is the choice of the configuration of the whole drivetrain, with a specific focus on the gearbox component, and afterward, each part is individually studied by the help of KISSsoft, a design software used to size, analyze and optimize machine elements and gearboxes.

4.1 Drivetrain configuration for the 22 MW offshore wind turbine

As mentioned in 2.1.3, the drivetrain is the “powerhouse” of the wind turbine, and it can differ from turbine to turbine. The choice of the correct configuration for the 22 MW is fundamental to optimizing the energy conversion by increasing the efficiency while keeping low costs and the weight of the device. Three possible structures of the drivetrain have been taken into account:

- Direct Drive
- Medium Speed
- High Speed

but only one is selected, which is the medium speed. The reasons behind this choice are multiple. From research on catalogs of well-known companies, it is possible to understand why currently the MS configuration is the most used one even though the trend is to push towards a DD drivetrain, at least for small wind turbines

since when it comes to high-power wind turbines, DD still requires more expensive and heavier generators [19]. If the HS brings significant technological benefits and the DD installation-cost benefits, the MS is the only one that can combine both advantages while being reliable, widely used, and commercialized. Plus, MS and HS have a high design voltage that helps to reach good values of efficiency with less effort due to the reduction of switching losses[20].

The MS drivetrain can further be divided into two big groups:

- 3-point suspension
- 4-point suspension.

The 3-point suspension drivetrain is supported by just one bearing at the rotor side. At the same time, the 4-point has an additional main bearing at the gearbox side, which isolates any non-torsional rotor loads upwind of the generator that could affect the gearbox reliability, decreasing the bearing life. Thus, the gearbox would be less sensitive to loads, permitting at the same time a reduction of its mass[21].

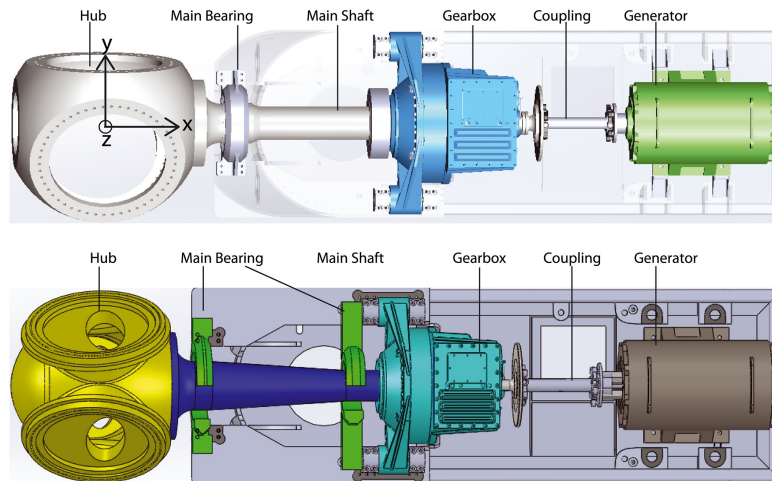


Figure 4.1: Three-point (top) and four-point (bottom) suspension drive train. Y. Guo, T. Parsons, K. Dykes, R.N. King: A systems engineering analysis of three-point and four-point wind turbine drivetrain configurations

For the 22 MW offshore wind turbine, the four-point drivetrain is the configuration selected.

4.2 The Gearbox

According to industry experience (see Winergy website [22]), gearboxes for MS drivetrains usually have 1 or 2 stages since the third one is generally for the HS.

Even though this configuration can decrease the failure rate at the HS part since it is not present, the gear ratio has to undergo a restriction where the maximum value that can be reached is 40 [23]. To avoid this issue, the most suitable solution is a 3-stage gearbox with two planetary and one parallel stage. The power-splitting gearbox is seen as a promising solution as well, but unfortunately, it is still not well developed.

Looking at the loads that the gearbox will endure during the operational condition, another but more expensive configuration is the 3-planetary stage gearbox, which helps to reduce the weight of the device further while keeping the torque density up.

Thus, the final choice is:

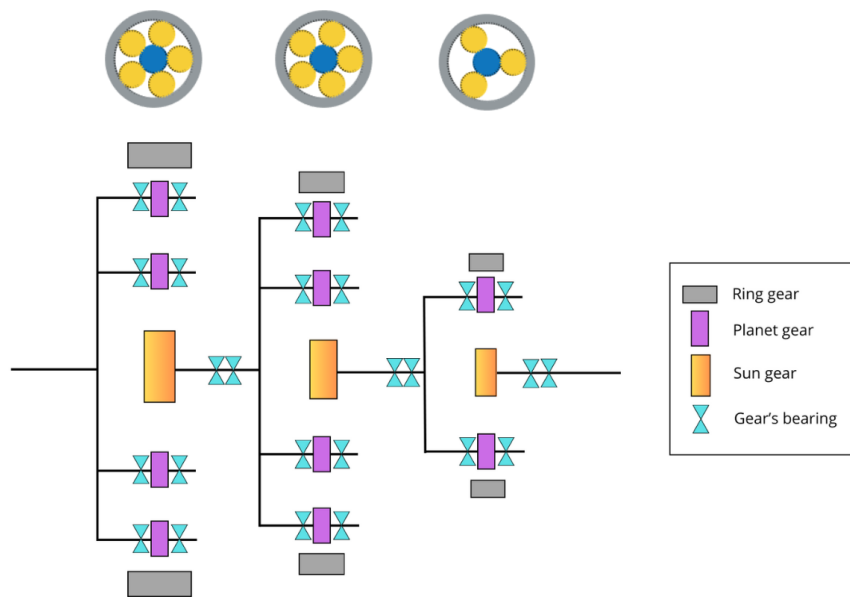


Figure 4.2: Gearbox configuration, with three planetary stages

The table 4.1 presents the 22 MW reference gearbox specification:

PARAMETER	VALUE
Type	Three planetary
First stage ratio	1:3.874
Second stage ratio	1:4.608
Third stage ratio	1:3.912
Total ratio	1:70
Designed power (MW)	22
Rated input shaft speed (rpm)	7
Rated generator shaft speed (rpm)	507.98
Rated input shaft torque (kNm)	52301.4
Rated generator shaft torque (kNm)	723.8
Service life (h)	150000

Table 4.1: 22MW reference gearbox specification.

How the gear ratio is selected? Been MS means that the output speed should be around 490 rpm, and since the rotor speed, which is also the input speed of the gearbox, is 7 rpm for the 22 MW wind turbine:

$$i = \frac{\text{input speed}}{\text{output speed}} = \frac{7}{490} = \frac{1}{70} \rightarrow 1 : 70 \quad (4.1)$$

4.2.1 Gears

The gearbox is composed of three planetary stages. Each stage has been designed following the same pathway, starting with some simple hand calculation, followed by using KISSsoft design software. The initial step consists of defining the input gear ratio for each stage so that the final product would be around 70 as measured in Eq.4.1. Actually, due to uncertainty that occurs during mathematical calculations, it is selected a restricted range for the gearbox ratio that goes from 65 up to 70. The input values are shown in table 4.1. It is essential to underline that the ratio for each stage should be a prime number or, even better, not an integer, and for medium-speed gearbox, it is recommended that the ratio should not be below 3 [24]. For the 22MW offshore wind turbine, the following hypothesis has been made:

- the ring gear is fixed $\rightarrow \omega_4 = 0$
- same module for each component of the same stage
- the axis of the planet gears are parallel.

Thus, for a planetary gear configuration, the nominal ratio is given by:

$$i = \frac{\omega_1}{\omega_3} = \frac{Z_1 + Z_4}{Z_1} \quad (4.2)$$

After manually defining the input parameter for each stage, KISSsoft is used. First, the entire first stage has been designed and fixed, moving then towards the second and lastly to the third. Opening the main page of KISSsoft, the planetary gear configuration is selected, and the input parameters are inserted, such as the input torque and speed, input gear ratio, helix angle, and the number of planets. The default material used for every gear has been kept unchanged, 18CrNiMO7-6. Afterward, the rough sizing is computed.

The first stage is run several times by changing the helix angle and the nominal ratio deviation. What is possible to observe is that the number of solutions that KISSsoft gives is always the same, five, and regarding the solutions themselves, it is seen that when it comes to the number of teeth, tip diameter, and pitch diameter, the numerical values are not subject considerable variation, but they are pretty the same. What really changes is the weight and partially the face width. The table presented below shows how, by increasing the helix angle, both the face width and the weight decrease.

PARAMETER	VALUE 1	VALUE 2
Helix angle (°)	8	7
Face width sun (mm)	822.2	830.3
Face width planet (mm)	797.2	805.0
Face width ring (mm)	826.4	830.3
Weight (Kg)	91145.5	93721.1

Table 4.2: Gear’s face width and weight variation due to different helix angle.

The final choice is merely linked to the lowest weight. Of course, the selected gears have been checked, and the final ratio, measured by hand calculation, is just less than 10% different from the input value, which is extremely good since the configuration chosen is well optimized. Using this new gear ratio, the output speed and torque are calculated and inserted as input parameters for the second stage.

In the second stage, the program is first run with a number of planets equal to 3. However, since the torque is still considerable, the obtained results show a non-optimized configuration: huge weight, almost doubled compared to the 5-planet stage, and the tip diameter of the ring more prominent than the first stage, which is not typical in gearboxes. Note that increasing the helix angle is another way to reduce the weight but with less effect than the number of planets. In this case, the possible solutions for the final design are multiple, and initially, three configurations are chosen. The first choice is mainly carried by three criteria: tip diameter smaller

than the first stage, low weight, and the number of teeth similar to the first stage to see how the variation in the torque and speed would change the gears. The first two criteria are also used for the second selection, which is also based on the ability to keep the gear dimensions close to the one of the first stage. The reason behind it is linked to the fact that this is a new technology, still not commercialized; therefore, it would be helpful for the production process if the dimensions were similar. An optimal gear ratio closest to the input one is the last criterion for choosing this configuration. Lastly, the nominal ratio deviation is changed, and few variations are observed except for a decrement in the tip diameter. Among these three selections, the one chosen is the second because the motivations behind it are the strongest ones, and the gear ratio is the closest to the one given as input, even though the variation is still significant.

For this reason, the input gear ratio for the third and last stage has to be changed according to the ones obtained in the first two stages. As done for the second stage, the input torque and speed are measured and inserted in KISSsoft. Since the torque is now way lower, a number of planets equal to three is the right choice. The nominal ratio deviation is put at five, leading to a decrement in the weight of the gears. Changing the helix angle is not fundamental for this part of the design since the dimensions are already good enough, but another run with a higher value for the angle is performed as well. The criterion to choose the best configuration is to find a good compromise between a high gear ratio within the range and a not-so-heavy device.

The last step before moving to the bearings and shaft design is to check and validate the choice for each stage. To do so, the final gear ratio is calculated by hand calculation, as well as the ratio between the number of teeth of the sun and ring gears and the number of teeth of the planet gear, which should never be an integer value. All the results are shown in Chapter 5.

Now, since the wind turbine operates at different speeds and loads throughout its lifetime, the gears must also be designed according to the fatigue analysis. The proceeding is the same as explained before. What changes is the input torque and power, which won't be the maximum value anymore but the load distribution got for the whole wind speed (see Chapter3), with their occurrences. Opening KISSsoft, in the "strength" section, instead of selecting torque and speed, the load spectrum is picked out, and the "own input" option is chosen; all the needed values are inserted. The rough sizing is run again, and the gears are selected by following the same criteria as before.

All the results are shown in Chapter 5.

Note that the gear design is not fixed until the bearings of the same stage are selected.

4.2.2 Bearings and Shafts

Once the gear configuration is defined, the bearings and shaft design can be initiated. KISSsoft designs bearings and shafts simultaneously in the section called "shaft calculation." For each stage, it is required to select the correct combination of bearings for the sun and planet gears, according to rating life and safety factors. It is also fundamental to look for a couple of bearings where at least one of them can bear the axial forces, if not both of them, while the other can take the radial one. Therefore, the best combinations can be chosen between [25]:

1. tapered roller bearing and cylindrical roller bearing
2. spherical thrust roller bearing and spherical roller bearing
3. spherical roller bearing and barrel-shaped roller bearing.

Then, after selecting one of the mentioned couples, it is necessary to understand which of the two bearings can take axial loads (if not both) and from which direction. In KISSsoft, the bearing that is able to take axial load is the one that has a very sharp angle between the two converging dotted lines shown in the pics down below, and the connecting point of them is far from the vertical axis of the bearing itself. This bearing can then be a fixed bearing adjusted on the left side or right side, depending on the direction where the axial loads are from. The direction of the loads is usually already defined in the software itself. Suppose that the bearing selected is fixed in the wrong direction: in this case, KISSsoft lets you know that thanks to a series of warnings and errors that can abruptly abort the software run, but it is also possible to notice it by looking at the results of the loads given as output. Sometimes, the bearing can stand axial load equally from both sides and then they can be fixed bearing adjusted on both sides, while the "radial bearing" is usually a non-locating. However, there are other criteria on which a couple of bearings can be chosen. Bearings can be [25]:

1. Self-aligning bearings which are able to compensate for misalignment within the bearing
2. Alignment bearings which can accommodate initial static misalignment
3. Rigid bearings that accommodate misalignment within the limits of their internal clearance.

and the choice should divert toward bearings that have the same functionality. Thankfully, the three pairs of bearings mentioned before are also compliant with this second requirement. The proceeding to design the planet gear is the same for each stage: initially, the gear-body shaft and a couple composed of a tapered roller bearing and a cylindrical roller bearing is selected. Cylindrical roller bearings

usually are used for radial loads while double-row tapered roller bearings can tolerate axial loads from both sides and radial loads. Following Figure 4.3, the double-row tapered roller bearing can just tolerate the axial loads. The next step is to size the bearings according to the rating life and safety factors that are presented as output parameters as well. Starting with massive bearings with an outer diameter slightly lower than the tip diameter of the gear, the first rough sizing is performed, and the results obtained will be fundamental to deciding to size down the bearing and to select the dimension to reduce. The lower the width, the lower the bearing capacity and thus the bearing life, while decreasing the diameter means to reduce the safety factor. Most probably, an extremely oversized configuration can be obtained, and then the size of the two bearings should be taken down until the rating life is higher than 130000 hours. Note that the rating life can also be changed by moving the bearings closer or further from the gear. When the final configuration is defined, the inner contour can be added. However, due to safety reasons, the diameter of the internal outline must not be higher than half of the external diameter of the gear-body shaft; this is the last criterion to follow during the choice of the design of the bearings.

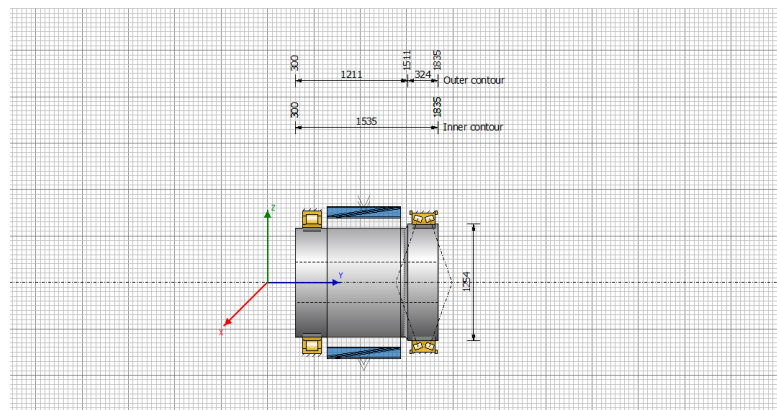


Figure 4.3: Planet gear's bearings configuration from KISSsoft, stage 1.

The sun gear is slightly more complicated. The first configuration selected consisted of four bearings, three on the left side and one on the right side. Nevertheless, this configuration had many issues: for example, despite the minimum rating life being archived by all the bearings, there was always one that showed a safety factor equal to 9999.9, which is not good. That is why the two bearings configuration is then searched. Now, for the sun gear, both the bearings are positioned on the right side. Fixed on the left or right side still depends on what is said. The couple chosen is primarily the spherical thrust roller bearing and spherical roller bearing, and the same proceeding done for the planet is now performed.

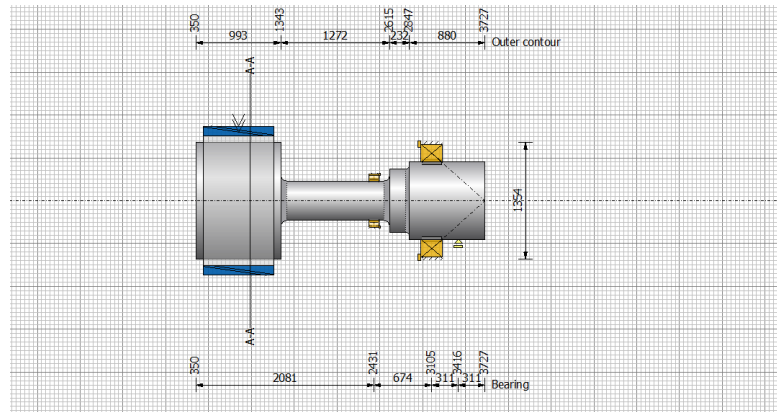


Figure 4.4: Sun gear's bearings configuration from KISSsoft, stage 1.

As it is possible to observe in the picture, another difference between the sun and planet gear is the additional presence of the support for the sun configuration, which is added because otherwise, the sum of the torque over the gear-body shaft would not be zero.

To conclude the discussion on how the bearing design is performed, a small note regarding the difference between L_{10h} and L_{nrh} must be explained. Both of them are considered while performing the selection, and while L_{10h} is the bearing rating life associated with mechanical loads, L_{nrh} is the bearing rating life considering other external factors as well, like lubrication or thermal loads. All the results are shown in Chapter 5.

Chapter 5

Results and Discussion

In this chapter, the outcomes of the processes reported in the previous two chapters of the thesis are shown through tables and images and then described, underlining the most significant results.

5.1 Global Analysis results

In this thesis section, the main results from Chapter 3 are reported and discussed.

5.1.1 Global Analysis: Location definition Outcomes

As already explained in Chapter 3, subsection 3.1, the location chosen to install the 22 MW wind turbine is 9 km from Bergen's coast. The results of the analysis performed by the contribution of MatLab are represented in the following graphics:

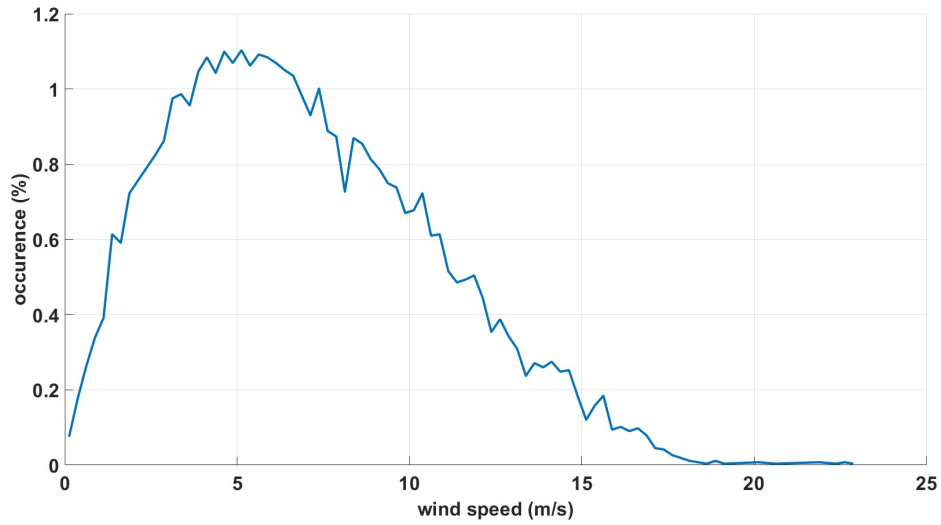


Figure 5.1: Occurrence of Wind Speed from Matlab

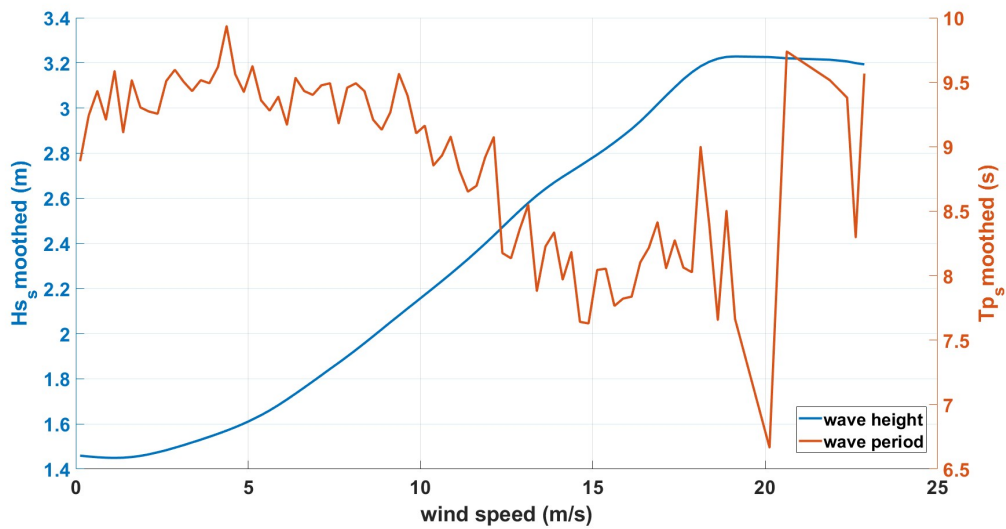


Figure 5.2: average sea state as a function of wind speed from Matlab

The first plot Fig.5.1, shows the trend and the occurrence of the wind speed in $\frac{m}{s}$ through the last four years (since 2019), for every month, day, and hour. As is it possible to observe, the most frequent velocity is around $5 \frac{m}{s}$, but it is likely to reach values close to $25 \frac{m}{s}$. Overall, it is possible to assert that the trend is exactly the one expected for a suitable location for a wind turbine, with a bell shape and the reach of values around $20 \frac{m}{s}$.

The second figure Fig.5.2, refers to the average sea state as a function of wind speed, where both the trend of wave height and period are displayed. For the 22 MW gearbox design, this plot is not used. However, it is fundamental for the choice of the location and further analysis regarding sea and wind loads necessary to design other components.

5.1.2 Global Analysis: Design Load Cases Outcomes

As described in the last section of Chapter 3, OpenFAST is run at different wind speeds. For each run, the value considered for the following step to design the gearbox is the rotor torque. At the same time, to check if the program is running correctly and no specific issues are occurring, the generator power, the blade pitch angle, the rotor speed, and bending moments are taken under control.

Note that the engineering approach over the gearbox design does not consider the first 100 seconds before the trend is set.

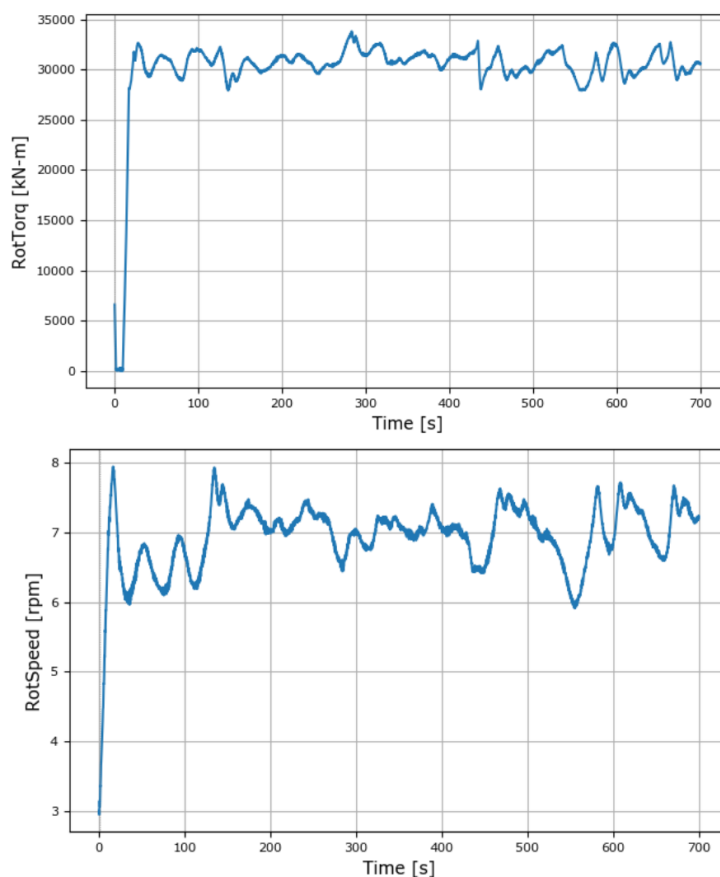


Figure 5.3: 12 m/s Rotor Speed and Torque as time function

The figure5.3 shows the torque trend for the rated speed of $12 \frac{m}{s}$. All the other results are shown in Appendix A.2. The stabilized trend of the torque seems to be present starting from a wind speed of $8 \frac{m}{s}$ where sudden drops can still be noticed; this might be caused by a decrement in the wind speed, which is not constant through the running due to turbulence. Below this wind speed value, the trend is slightly different since the wind is not strong enough to permit it to reach those conditions. However, some issues can be seen after a wind speed of $18 \frac{m}{s}$, where the plots start to show an odd trend with portions of resonance:

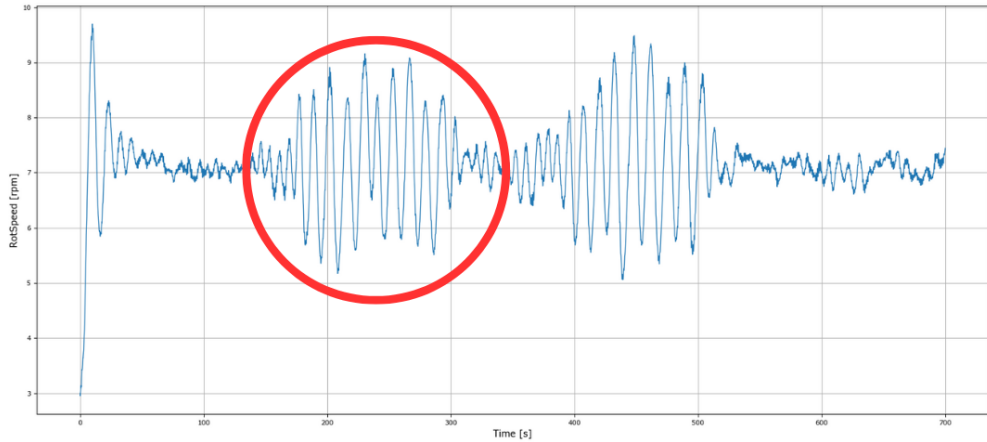


Figure 5.4: 22 m/s Rotor Speed Resonance

That might be caused by the controller, which is still not well-performing when it comes to high wind speed, and since the 22 MW wind turbine model is still in its preliminary analysis, this could be considered perfectly normal. Plus, as shown in Fig.5.1 20, 22 and $24 \frac{m}{s}$ do not occur frequently; their occurrence is almost close to 0%. Lastly, despite the resonance in some portions of the plots, the overall trend is similar to the $18 \frac{m}{s}$, mainly for the parameters that should be used for the design. Thus, it is decided to run the program with a wind speed of $19 \frac{m}{s}$ by changing the RandSeed number.

5.2 Local Analysis results

After gathering all the data for loads and wind speeds, the design of the gearbox components can start, and this section presents the results obtained from KISSsoft,

beginning from the gears and moving toward bearings and shafts.

5.2.1 Local Analysis: Gears Outcomes

The gears have been designed for both ultimate strength and fatigue analysis, whose results are compared, starting from the first stage up to the last one. The table inserted in this subsection presents the most important values for the discussion; all the other parameters of each gear stage are placed in Appendix A.3.

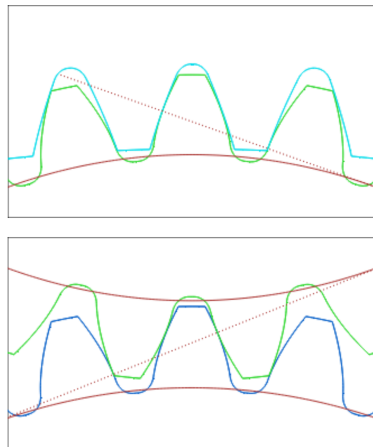


Figure 5.5: Planet-sun gear meshing and the planet-ring meshing, stage 1, from KISSsoft



Figure 5.6: 2-D configuration of stage 1 from KISSsoft

The first image represents the planet-sun gear meshing and the planet-ring meshing, while the last is the 2-D configuration of stage 1.

STAGE 1	FA	US
Module (mm)	50	50
N. of teeth sun	32	32
N. of teeth planet	30	30
N. of teeth ring	93	93
Face width sun (mm)	822.2	801.1
Face width planet (mm)	797.2	776.1
Face width ring (mm)	826.4	819.8
Weight (Kg)	91145.6	88852.9
Output Gear ratio	3.906	3.906

Table 5.1: Stage 1, gears main parameters obtained from Fatigue and Ultimate Strength analysis.

Looking at the results obtained from the two analyses, the first stage seems static, and the main outputs are very similar. This condition can also be seen if other input parameters, such as the helix angle or the gear ratio deviation, change. The weight is one of the few results that significantly vary; a slight increment of it involves the gears designed according to the Fatigue analysis, as expected, due to a wider width that reaches values close to 1 meter. Since the system works at very high power, such numbers are the norm, considering at the same time that it is still a preliminary analysis. Alongside the variation of the helix angle, another way to decrease the weight, which can be further studied, is to choose a configuration of seven planets instead of five.

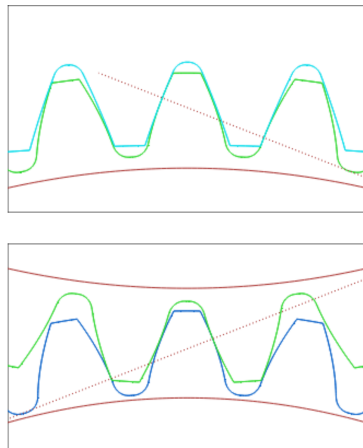


Figure 5.7: Planet-sun gear meshing and the planet-ring meshing, stage 2, from KISSsoft



Figure 5.8: 2-D configuration of stage 2 from KISSsoft

The first image represents the planet-sun gear meshing and the planet-ring meshing, while the last is the 2-D configuration of stage 2.

STAGE 2	FA	US
Module (mm)	28	28
N. of teeth sun	38	39
N. of teeth planet	47	47
N. of teeth ring	132	136
Face width sun (mm)	467.7	419.6
Face width planet (mm)	452.4	404.4
Face width ring (mm)	467.7	419.6
Weight (Kg)	33145.1	29930.7
Output Gear ratio	4.474	4.487

Table 5.2: Stage 2, gears main parameters obtained from Fatigue and Ultimate Strength analysis.

The design of the second stage for the fatigue is slightly different compared to the ultimate strength, but no significant changes have been involved. As for the first stage, the weight is increased due to a bigger teeth width, but on the contrary, while the gear ratio of the first stage is kept the same, here it is possible to observe a slight change in the output value, and that will have consequences for the third stage because the input load cases will be different, compared to the one obtained from the gear ratio measured by hand calculations.

An important note for this stage is the number of planets: the first run was performed with three planets, but the outcomes were not suitable because, as a consequence of a very significant torque, the tip diameter of the ring was higher than the one of the first stage and also the total weight was higher than expected.

The first two stages are initially run with a helix angle of 10° , but to optimize the configuration and make it lighter and smaller, the helix angle is decreased to 8° .

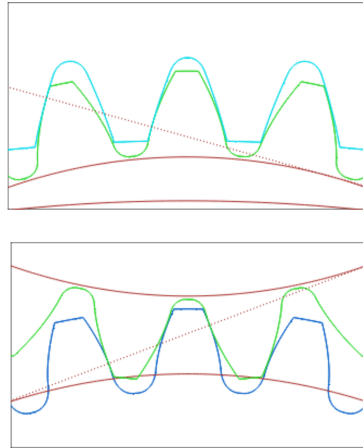


Figure 5.9: Planet-sun gear meshing and the planet-ring meshing, stage 3, from KISSsoft



Figure 5.10: 2-D configuration of stage 3 from KISSsoft

The first image represents the planet-sun gear meshing and the planet-ring meshing, while the last is the 2-D configuration of stage 3.

STAGE 3	FA	US
Module (mm)	22	22
N. of teeth sun	34	34
N. of teeth planet	31	31
N. of teeth ring	98	98
Face width sun (mm)	352.1	334.9
Face width planet (mm)	338.6	321.3
Face width ring (mm)	352.1	334.9
Weight (Kg)	6019.4	5592.3
Output Gear ratio	3.882	3.882

Table 5.3: Stage 3, gears main parameters obtained from Fatigue and Ultimate Strength analysis.

Despite the input load cases being different from fatigue to ultimate strength, the final configuration of the third stage does not undergo significant changes, and the output gear ratio is kept the same. The main differences are still in the weight and the teeth' width. However, this design is not the final one; after the definition of bearings and shafts, the axial loads that the third stage has to face are bigger than expected, and to decrease them, the helix angle should be reduced from 8° and put at 4° . The table shows the final values of the actual third stage:

STAGE 3	FA
Module (mm)	28
N. of teeth sun	26
N. of teeth planet	24
N. of teeth ring	74
Weight (Kg)	6241.1
Output Gear ratio	3.923

Table 5.4: Stage 3, gears main parameters when the helix angle is equal to 4°

Note that a lighter and smaller design followed by a high gear ratio is the one that is usually optimized.

5.2.2 Local Analysis: Shaft and Bearing Outcomes

The final step to conclude the design of the gearbox for the 22 MW wind turbine is the design of the bearings and shafts of all the stages. The proceeding is described in Chapter4, while in this section, the most important outcomes are presented and discussed.

Since designing the sun and planet's bearing is the same for all the stages, the discussion will be carried on generically. The specific results (tables and pictures) of all the stages are inserted in Appendix A.3.

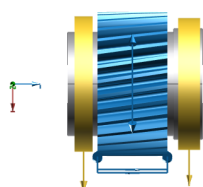


Figure 5.11: Configuration for a planet gear.

Fig. 5.11 shows a typical configuration for a planet gear. The gearbody is bored in its center to host the gear shaft connecting element. As mentioned, this diameter should not exceed half of the outer diameter because the closer to this value, the higher the risk of failure. Nevertheless, the high loads from the wind reduce the availability to choose smaller bearings than the one selected, where even a variation of 5% in the width or the diameter of the bearing can drop the rating life below the established minimum value of 130000 hours. A small note for the L_{nhr} : usually, it should be higher than L_{h10} , but sometimes it can be 0 due to the lack in the software of some geometry details for that peculiar bearing. What matters is that when L_{nhr} is different from 0, it should not be much lower than the value of L_{h10} .

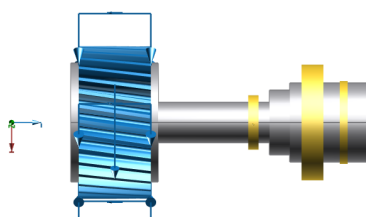


Figure 5.12: Configuration for a sun gear.

The sun gear tends to be overdesigned, mainly in the third stage. However, more miniature bearings weren't possible to select because the shaft diameter must

be high enough to host the connecting elements inside (usually another shaft), whose diameters are typically around 150-200 mm. On the right side, the space left from the gear to the first bearing is to host the gear spline. One of the most significant drawbacks of planetary gears is the elastic deformation that occurs during operating conditions. Therefore, it is necessary to optimize the load-sharing within the components of the planetary gearboxes. There are three methods to improve in this direction with their advantages and disadvantages:

- creates a flexible ring gear as in the Stoeckicht design
- uses flexible pins to support planet gears to make them adjustable to shape and load variation
- has a floating sun gear

This last method is the easiest and most common one, and that is why it is chosen even though it is not suitable for gearboxes with a number of planets higher than three. However, since this design is entirely new, using something already approved and commercialized is the right direction for now. For sure, once the design is finalized, the choice should divert toward one of the first two options [26]. It is still unknown why, if the position of the bearing is inverted, the configuration is not working anymore: KISSsoft aborts the run, and no results are returned.

Chapter 6

Conclusion

The increase in the energy demand, alongside the need to search for new and more advanced renewable sources, leads to progress in the wind energy field, with the building of more powerful turbines, onshore and offshore.

In this thesis, the design of a 22 MW gearbox for offshore wind turbines was presented. This is one of the first detailed design works in this power range that has been carried out. The gearbox for the 22MW offshore wind turbine is still in its preliminary analysis, and a rough design has been performed using peculiar software able to gather wind loads and create a satisfying initial configuration. The study is based on a three-stage planetary gearbox, where each gear and bearing is analyzed and designed according to Fatigue and Ultimate Strength analysis. The modeling is carried out in KISSsoft, after getting the necessary wind data from OpenFAST.

The results obtained for the gears and bearings present some good points and drawbacks that lead to the following conclusion:

1. The global analysis is fundamental for having a brief overview regarding the wind loads and the possible size of the wind turbine. It also defines the possible location for the installation of the turbine, which, in this thesis, is around 9 Km from Bergen's shore.
2. The highest torque that a turbine can experience in its lifetime is estimated to be around 52301.4 KNm. This value is obtained from the global analysis performed by using OpenFAST software and the IEC standards, and it represents an important starting point because it helps to understand how high loads from the wind are one of the main reasons behind the overdesign condition of some gearbox components, like the right bearing of the sun, stage 3, where the rating life is above 1000000.
3. The total weight of the gearbox, except for housing, is 130.5 tons and can be

decreased by adding the seven-planet configuration in the first stage or by changing the helix angle in each stage, paying attention at the same time to the gear ratio and the efficiency of the gears.

4. Despite the overdesign and some issues in the wind data gathering due to the defective controller of OpenFAST, the results shown in Appendix A can be considered satisfying if compared to the design of the gearbox of the 10 and 15 MW offshore wind turbine: the components are more considerable and heavier, but the differences are not that excessive.
5. The modeling, according to Fatigue or Ultimate Strength analysis, does not change much the main features of the gears. However, it is essential to perform both due to the variability of the wind conditions and the sudden peak in the torque that the turbine can undergo.
6. Overall, is it possible to assert that the MS gearbox with three planetary stages is a good choice for an initial configuration due to its compactness and ability to work at high loads and variable conditions.

Further studies will be devoted to a more optimized design while adjusting and updating OpenFAST for the 22 MW offshore wind turbine, which unfortunately showed some problems during the data gathering because of the controller, which is still defective. It is recommended to optimize the first stage, making it lighter and smaller with a seven-planet configuration. The studies should also divert toward the design of gearbox housing, the connection elements between the stages, and the manufacturing of new bearings more suitable for high-power turbines.

Appendix A

Appendix A

A.1 Wind turbine Siting

Siting: ERAFIVEDats-extraction

```
1 %   DOWNLOAD data from https://cds.climate.copernicus.eu/cdsapp#!/
   dataset/reanalysis-era5-single-levels?tab=form
2
3 % Product type:
4 %   Reanalysis
5 % Variables:
6 %   100m u-component of wind (u100)
7 %   100m v-component of wind (v100)
8 %   Significant height of combined wind waves and swell (Hs)
9 %   Peak wave period (Tp)
10 %  Mean wave direction (Dirn)
11 % Years:
12 %   2020 and 2021
13 % Month:
14 %   all
15 % Days:
16 %   all
17 % Time:
18 %   all
19 % Geographical area:
20 %   Sub-region extraction
21 %       North-> north coordinate of the center of the cell (
   example1:37^o example2: 12.5^o)
22 %       West-> west coordinate of the center of the cell (example1
   :20^o example2: -9.5^o)
23 %       South-> south coordinate of the center of the cell plus
   0.1^o (example1:36.9^o example2: 12.4^o)
```

```

24 %           East-> east coordintate of the center of the cell plus 0.1^
      o (example1:20.1^o example2: -9.4^o)
25 %
26 % Output: ScatterWaveAndWind = (N x 4) : Significant wave height ,
      Peak period , Wind speed , Occurrence
27 %
28 % This script reads and analyzes a single geographical data point
29 %%
30 clearvars %
      Delete old variables
31 close all %
      Close old figures
32 clc %
      Clear Command Window
33 addpath('Functions') %
      Add the path to the folder Funcions
34
35 %% Adapt the script to the case study
36
37 %Begen_site
38 name_file = 'Bergen.nc'; % Exactly the
      name of the file to be uploaded
39 name_site = 'Bergen'; %
      Arbitrary, but meaningful!
40 year_range = '2019_2021'; %
      Arbitrary, but meaningful!
41 year_start = 2019; %
      Year start
42 n_year = 3; %
      Number of consecutive years
43
44 %% Data desired
45 data_desired.Hs = 1; %
      Flag: do I read the significant wave height?
46 data_desired.Tp = 1; %
      Flag: do I read the energy period (mean wave period)?
47 data_desired.u100 = 1; %
      Flag: do I read the u component of the wind at 10m a.s.l.?
48 data_desired.v100 = 1; %
      Flag: do I read the v component of the wind at 10m a.s.l.?
49 data_desired.Dirm = 1; %
      Flag: do I read the mean direction?
50 data_desired.dateTime = 1; %
      Flag: do I read the time stamp?
51 data_desired.Lat_Long = 1; %
      Flag: do I read the Latitude and Longitude?
52 savedflag = 0; %
      Flag: is it already saved?

```

```

53 data_source          = 'ERA5';                                %
   Arbitrary: source of the dataset
54 nLon                = 1;                                    %
   Index of the Longitude vector to be analysed
55 nLat                = 1;                                    %
   Index of the Latitude vector to be analysed
56
57 %% Data extraction from the nc file
58 [Data]              = WaveAndWind_data_extraction_ECMWF_WOEP2022_FNC(
   name_file, name_site, year_range, data_desired, savedflag,
   data_source, nLon, nLat);
59 Data.name_site      = name_site;
60 Data.year_start     = year_start;
61 Data.n_year         = n_year;
62
63 %% Wave rose plot
64 figure()
65 rose_plot_FNC(Data.Dir, Data.Hs, 'dtype', 'meteo', 'umisura', '', '
   parametro', 'H_s', 'di', [0:round(max(Data.Hs)/5,1):max(Data.Hs)], 'n'
   ,24, 'lablegend', '[m]', 'labtitle', '');
66
67 Wind rose plot
68 figure()
69 rose_plot_FNC(Data.dir, Data.v, 'dtype', 'meteo', 'umisura', '', 'parametro
   ', 'v', 'di', [0:round(max(Data.v)/5,1):max(Data.v)], 'n', 24, '
   lablegend', '[m/s]', 'labtitle', '');
70
71 %% Occurrences and Energy scatter
72 dHs = 0.25;
73 dTp = 0.25;
74 [occ_1d energy_1d Hs_mat_int Tp_mat_int] =
   Scatter_OCC_POW_1D_WOEP2022_FNC(Data.Hs, Data.Tp, -1, 1, dHs, dTp, 1, 1);
75
76 %% WaveAndWind Occurrences
77 dv=0.25;
78 dHs = 0.25;
79 dTp = 0.25;
80 ScatterWaveAndWind=Scatter_OCC_3D_WaveAndWind_WOEP2022_FNC(Data, dv,
   dHs, dTp)
81
82 %%
83 % figure(6)
84 figure(5)
85 figure(4)
86 figure(3)
87 figure(2)
88 figure(1)
89 %% Save data
90 save(['triplet_' name_site '_full'], 'ScatterWaveAndWind')

```

Siting: Simplify-triplet

```

1  clf
2  load(['triplet_Bergen_full.mat']);
3  [B,I] = sort(ScatterWaveAndWind(1:7198,3));
4  DataSave=sort(ScatterWaveAndWind(I,:),3);
5  [C,ia,ic] = unique(DataSave(:,3));
6  wind=C; % wind speed only
7  occ=zeros(length(C),1); %occurrency of wind speed
8  for i=1:length(ic)
9      occ(ic(i))=occ(ic(i))+DataSave(i,4)
10 end
11 % evaluation of mean,max,min,deviation
12 % of the wave height and period
13 % for each wind speed
14 Hs=zeros(length(C),1);
15 Hsdev=zeros(length(C),1);
16 Hsmax=zeros(length(C),1);
17 Hsmin=zeros(length(C),1);
18 Tp=zeros(length(C),1);
19 for i=1:length(wind)
20     if i<length(wind)
21         h=ia(i):(ia(i+1)-1);
22         Hs(i)=sum(DataSave(h,1).*DataSave(h,4))/sum(DataSave(h,4));
23         Hsdev(i)=std(DataSave(h,1),DataSave(h,4));
24         Hsmax(i)=max(DataSave(h,1));
25         Hsmin(i)=min(DataSave(h,1));
26         Tp(i)=sum(DataSave(h,2).*DataSave(h,4))/sum(DataSave(h,4));
27     else
28         Hs(i)=sum(DataSave(ia(i):end,1).*DataSave(ia(i):end,4))/sum(
DataSave(ia(i):end,4));
29         Hsdev(i)=std(DataSave(ia(i):end,1),DataSave(ia(i):end,4));
30         Hsmax(i)=max(DataSave(ia(i):end,1));
31         Hsmin(i)=min(DataSave(ia(i):end,1));
32         Tp(i)=sum(DataSave(ia(i):end,2).*DataSave(ia(i):end,4))/sum(
DataSave(ia(i):end,4));
33     end
34 end
35
36
37  clf
38  % plot the occurrency of wind speed
39  hold on
40  set(gca,"FontSize",25,"FontWeight","bold")
41  ax.FontSize=25;
42  plot(wind,(occ)*100,"LineWidth",3)
43
44  xlabel("wind speed (m/s)","FontSize",25,"FontWeight","bold")

```

```

45 ylabel("occurence (%)", "FontSize",25,"FontWeight","bold")
46 grid on
47
48 clf
49 hold on
50 set(gca,"FontSize",25,"FontWeight","bold")
51
52 % Smooth input data
53 Hs_smoothed = smoothdata(Hs,"gaussian","SmoothingFactor",0.09999999999999998);
54 yyaxis left
55 plot(wind,Hs_smoothed,"LineWidth",3)
56 ylabel("Hs_smoothed (m)")
57 hold off

```

A.2 Global Analysis

OpenFAST results for rotor torque:

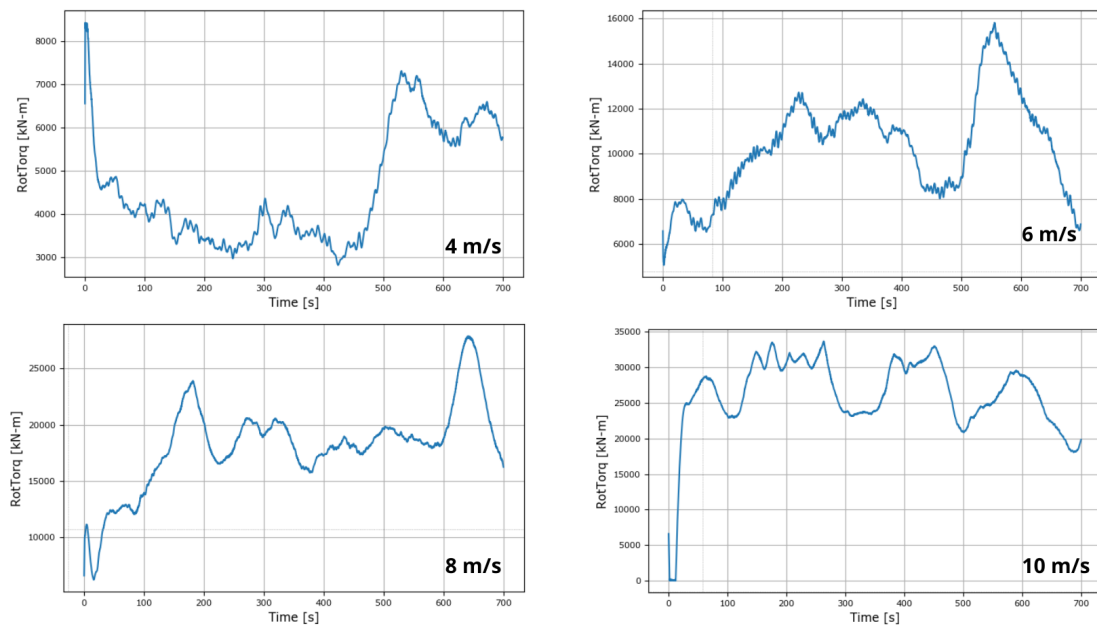


Figure A.1: Rotor Torque for 4,6,8 and 10 m/s wind speed, from OpenFAST.

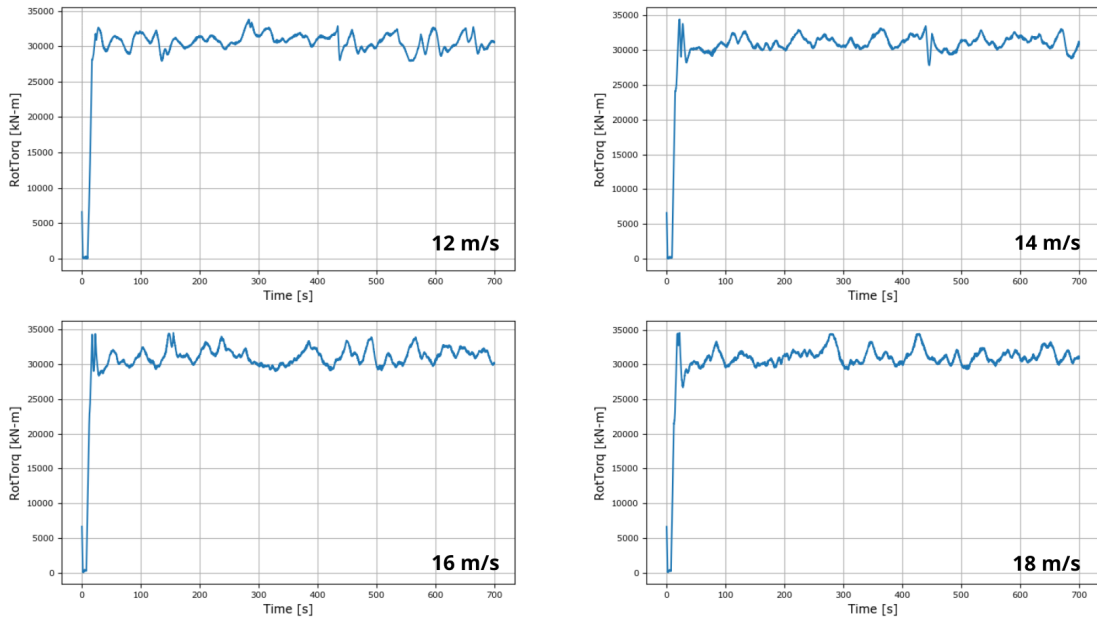


Figure A.2: Rotor Torque for 12,14,16 and 18 m/s wind speed,from OpenFAST.

LDD for each wind speed:

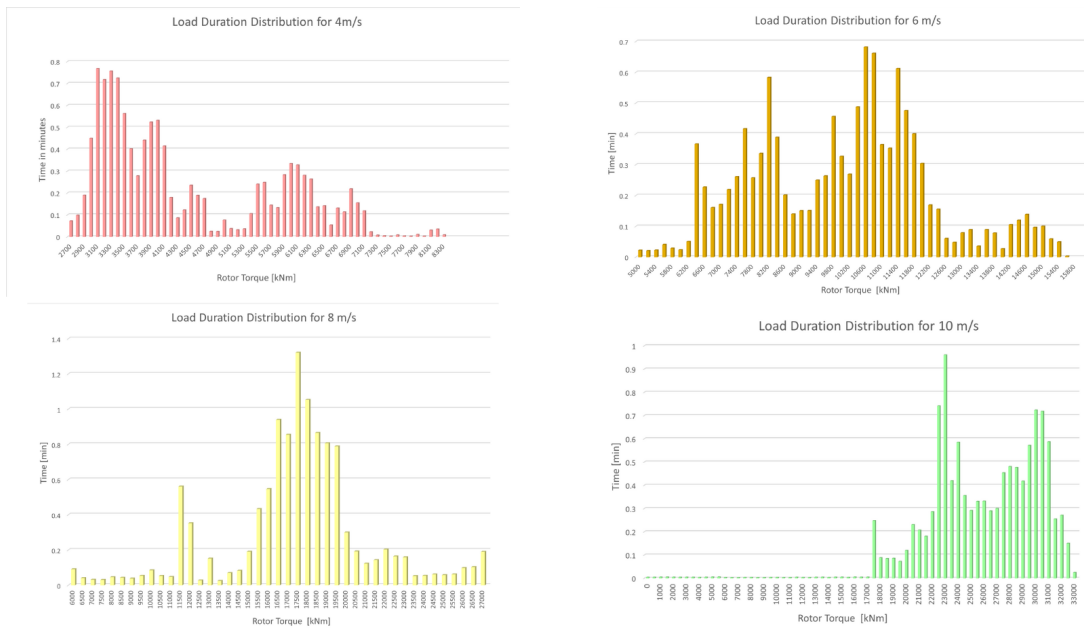


Figure A.3: LDD for 4,6,8 and 10 m/s wind speed.

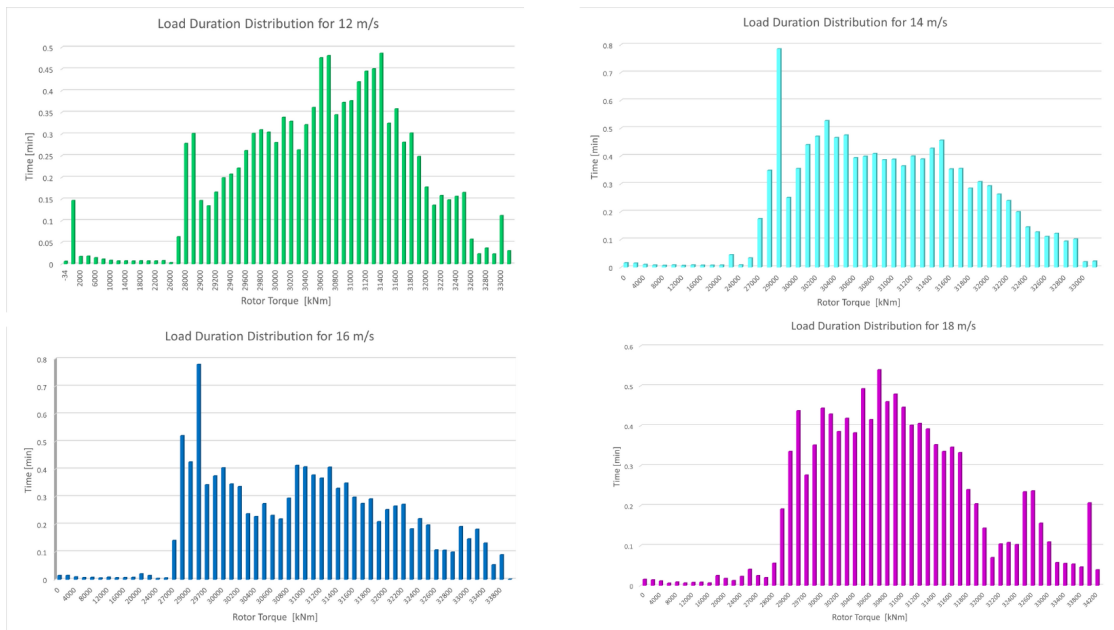


Figure A.4: LDD for 12,14,16 and 18 m/s wind speed.

Weibull Distribution Script:

```

1 close all
2 clc
3
4 Velocity = [0:2:24];
5 L = length(Velocity);
6 n = 1;
7 k = 1.708;
8 c = 8.526;
9 occurrence = [0.02137 0.06941 0.10325 0.10598 0.08697 0.0696 0.04409
10              0.02546 0.01158 0.00207 0.000502 0.000564171 0];
11 for n =1:L
12     i(n) = Velocity(n);
13     We(n) = (k/c)*(i(n)/c)^(k-1)*exp(-(i(n)/c)^k);
14     n = n+1;
15 end
16 hold on
17 title('Weibull Distribution for Wind Speed', 'FontSize',15)
18 bar(Velocity, occurrence, 'yellow')
19 f = plot(Velocity, We, 'b', LineWidth = 2)
20 xlabel("Wind speed (m/s)", "FontSize",15)
21 ylabel("Density (%)", "FontSize",15)
22

```

```
23 grid on
24 A = trapz (Velocity , We)
```

Ultimate Load Script:

```
1 clear all
2 close all
3 clc
4
5 A = [34571.139
6 34566.304
7 34598.938
8 34577.594
9 34648.92
10 34688.423
11 33968.496
12 34537.231
13 34541.453
14 34654.239
15 34585.617
16 346074.59
17 34654.042
18 34640.1656
19 34876.5892
20 34557.5542
21 34651.8216
22 34631.7683
23 34626.6873
24 34563.6939
25 ];
26
27 pd = fitdist(A, 'ev');
28
29 cdf(pd,A)
```

LDD for the whole wind range Script:

```
1 close
2
3 clear
4
5 clc
6
7
8
9 n = 10;
10
```

```
11 T_frac = zeros(12,n);
12
13
14
15 for k = 1:10
16
17     i = 2*k+1;
18
19     V = i;           % wind speed m/s
20
21     TITLE = sprintf('NIM wind speed %g m/s',V);
22
23     Link = sprintf('Loads and Wind\\NIM_%g.txt',V);
24
25
26     DATA = readmatrix(Link);
27
28
29     T_H = histogram(DATA(:,2),0:35e3/n:35e3);
30
31     T_num = T_H.BinCounts;
32
33     T_frac(k,:) = T_num*0.01/60/10;      % fraction of 10-min
34
35 end
36
37
38
39 xlabel('Torque (kNm)')
40
41 ylabel('Number of load in 10-minutes data')
42
43 title(TITLE)
44
45
46
47 Rec = readmatrix('Loads and Wind\\Recurrence.txt');
48
49 rec = zeros(10,1);
50
51 for k = 1:12
52
53     i = 2*k+1;
54
55     switch i
56
57         case 3
58
59             av = Rec(1,2)+Rec(2,2)/2;
```

```
60
61     case 25
62         av = Rec(23,2)+Rec(22,2)/2;
63
64     otherwise
65         av1 = find(Rec(:,1)==i);
66         av = Rec(av1,2)+Rec(av1-1,2)/2+Rec(av1+1,2)/2;
67
68     end
69     rec(k) = av;
70
71 end
72
73 Bin_val = 0:35e3/n:35e3;
74
75 T_fr = T_frac'*rec/sum(T_frac'*rec);
76
77 T_LDD = [Bin_val(2:end)' T_fr];
78
79 bar(T_LDD(:,1),T_LDD(:,2))
```

A.3 Local Analysis

First stage gears:

STAGE 1	VALUE for LDD	VALUE for ULTIMATE LOAD
N. of planet gear	5	5
Input Speed (rpm)	7	7
Output speed (rpm)	27.118	27.118
Input Gear ratio	3.874	3.874
Output Gear ratio	3.90625	3.90625
Pressure angle (°)	20	20
Helix angle (°)	8	8
Module (mm)	50	50
N. of teeth sun	32	32
N. of teeth planet	30	30
N. of teeth ring	93	93
Face width sun (mm)	822.2	801.1
Face width planet (mm)	797.2	776.1
Face width ring (mm)	826.4	819.8
Tip diameter sun (mm)	1736.5	1733.9
Tip diameter planet (mm)	1637.7	1635.1
Tip diameter ring (mm)	4614.8	4607.7
Weight (Kg)	91145.6	88852.9
Efficiency	0.995	0.995

Table A.1: Specification for stage 1, gears.

Second stage gears:

STAGE 2	VALUE for LDD	VALUE for ULTIMATE LOAD
N. of planet gear	5	5
Input Speed (rpm)	27.118	27.118
Output speed (rpm)	121.3	121.7
Input Gear ratio	4.608	4.608
Output Gear ratio	4.474	4.487
Pressure angle (°)	20	20
Helix angle (°)	8	8
Module (mm)	28	28
N. of teeth sun	38	39
N. of teeth planet	47	47
N. of teeth ring	132	136
Face width sun (mm)	467.7	419.6
Face width planet (mm)	452.4	404.4
Face width ring (mm)	467.7	419.6
Tip diameter sun (mm)	1142	1145.6
Tip diameter planet (mm)	1393.4	1400.4
Tip diameter ring (mm)	3706.4	3733.6
Weight (Kg)	33145.1	29930.7
Efficiency	0.996	0.996

Table A.2: Specification for stage 2, gears.

Third stage gears:

STAGE 3	VALUE for LDD	VALUE for ULTIMATE LOAD
N. of planet gear	3	3
Input Speed (rpm)	121.3	121.7
Output speed (rpm)	470.6	472.4
Input Gear ratio	4.01	3.912
Output Gear ratio	3.882	3.882
Pressure angle (°)	20	20
Helix angle (°)	8	8
Module (mm)	22	22
N. of teeth sun	34	34
N. of teeth planet	31	31
N. of teeth ring	98	98
Face width sun (mm)	352.1	334.8
Face width planet (mm)	338.6	321.3
Face width ring (mm)	352.1	334.8
Tip diameter sun (mm)	788	777
Tip diameter planet (mm)	749.9	740.4
Tip diameter ring (mm)	2115.9	2092.8
Weight (Kg)	6019.4	5592.3
Efficiency	0.994	0.994

Table A.3: Specification for stage 3, gears..

STAGE 3	VALUE
N. of planet gear	3
Input Speed (rpm)	121.3
Output speed (rpm)	475.8
Input Gear ratio	4.01
Output Gear ratio	3.923
Pressure angle (°)	20
Helix angle (°)	4
Module (mm)	28
N. of teeth sun	26
N. of teeth planet	24
N. of teeth ring	76
Face width sun (mm)	351.5
Face width planet (mm)	336.3
Face width ring (mm)	351.5
Tip diameter sun (mm)	769.6
Tip diameter planet (mm)	750.4
Tip diameter ring (mm)	2054.2
Weight (Kg)	6241.1
Efficiency	0.994

Table A.4: Stage 3 and Helix angle equal to 4°, specifications from LDD analysis.

First-stage bearings specifications:

BEARING DESIGN	STAGE 1 SUN (LEFT)	STAGE 1 SUN (RIGHT)	STAGE 1 PLANET (LEFT)	STAGE 1 PLANET (RIGHT)
MAX. DEFLECTION	1357.9 μm	1357.9 μm	508 μm	508 μm
MAX. STRESS	$1226.6 \frac{N}{\text{mm}^2}$	$1226.6 \frac{N}{\text{mm}^2}$	$4.68 \frac{N}{\text{mm}^2}$	$4.68 \frac{N}{\text{mm}^2}$
EQUIVALENT STRESS				
MAX. BEARING LIFE STATIC	430017.08 h	430017.08 h	553733.3 h	553733.3 h
BEARING SAFETY	15.26	15.26	15.97	15.97
S0 - SAFETY FACTOR	25.26	15.26	15.97	19.19
L10H	199266 h	580558 h	622199 h	553733.3 h
INNER DIAMETER	900 mm	460 mm	1180 mm	1250 mm
OUTER DIAMETER	1320 mm	620 mm	1540 mm	1500 mm
NOMIAL WIDTH	621 mm	118 mm	206 mm	250 mm
TYPE OF BEARING	Fixed bearing adjusted on the left	Fixed bearing adjusted on the right	Non-locating bearing	Fixed bearing adjusted on both sides
TYPE	Spherical roller thrust bearing	Spherical roller bearing	Cylindrical roller bearing (single row)	Tapered roller bearing (paired)(O,TDO)

Table A.5: Stage 1, bearings specification.

Second-stage bearings specifications:

BEARING DESIGN	STAGE 2 SUN (LEFT)	STAGE 2 SUN (RIGHT)	STAGE 2 PLANET (LEFT)	STAGE 2 PLANET (RIGHT)
MAX. DEFLECTION	511.9 μm	511.9 μm	350.9 μm	350.9 μm
MAX. STRESS	$418.7 \frac{N}{\text{mm}^2}$	$418.7 \frac{N}{\text{mm}^2}$	$3.99 \frac{N}{\text{mm}^2}$	$3.99 \frac{N}{\text{mm}^2}$
EQUIVALENT STRESS				
MAX. BEARING LIFE STATIC	261743 h	261743 h	143554.1 h	143554.1 h
BEARING SAFETY	32.7	32.7	19.61	19.61
S0 - SAFETY FACTOR	37.4	32.7	19.61	26.16
L10H	201973 h	658883 h	249208 h	808713 h
INNER DIAMETER	600 mm	400 mm	1000 mm	723 mm
OUTER DIAMETER	900 mm	500 mm	1220 mm	914 mm
NOMIAL WIDTH	180.2 mm	75 mm	128 mm	187.3 mm
TYPE OF BEARING	Fixed bearing adjusted on the left	Fixed bearing adjusted on the right	Non-locating bearing	Fixed bearing adjusted on both sides
TYPE	Spherical roller thrust bearing	Spherical roller bearing	Cylindrical roller bearing (single row)	Tapered roller bearing (paired)(O,TDO)

Table A.6: Stage 2, bearings specification.

Third-stage bearings specifications:

Appendix A

BEARING DESIGN	STAGE 3 SUN (LEFT)	STAGE 3 SUN (RIGHT)	STAGE 3 PLANET (LEFT)	STAGE 3 PLANET (RIGHT)
MAX. DEFLECTION	421.2 μm	421.2 μm	203.7 μm	203.7 μm
MAX. EQUIVALENT STRESS	210.2 $\frac{\text{N}}{\text{mm}^2}$	210.2 $\frac{\text{N}}{\text{mm}^2}$	9.08 $\frac{\text{N}}{\text{mm}^2}$	9.08 $\frac{\text{N}}{\text{mm}^2}$
MAX. BEARING LIFE STATIC	314621.2 h	314621.2 h	184720.55 h	184720.55 h
BEARING SAFETY SO - SAFETY FACTOR	56.35	56.35	20.26	20.26
L10H	59.08	56.35	20.26	25.72
INNER DIAMETER	170331 h	>1000000	175231 h	335672 h
OUTER DIAMETER	460 mm	320 mm	400 mm	347.7 mm
NOMIAL WIDTH	620 mm	400 mm	600 mm	469.9 mm
TYPE OF BEARING	95 mm	60 mm	118 mm	138.1 mm
TYPE	Fixed bearing adjusted on the left Spherical roller thrust bearing	Fixed bearing adjusted on the right Spherical roller bearing	Non-locating bearing Cylindrical roller bearing (single row)	Fixed bearing adjusted on both sides Tapered roller bearing (paired)(X,TDI)

Table A.7: Stage 3, bearings specification.

Final configuration design:

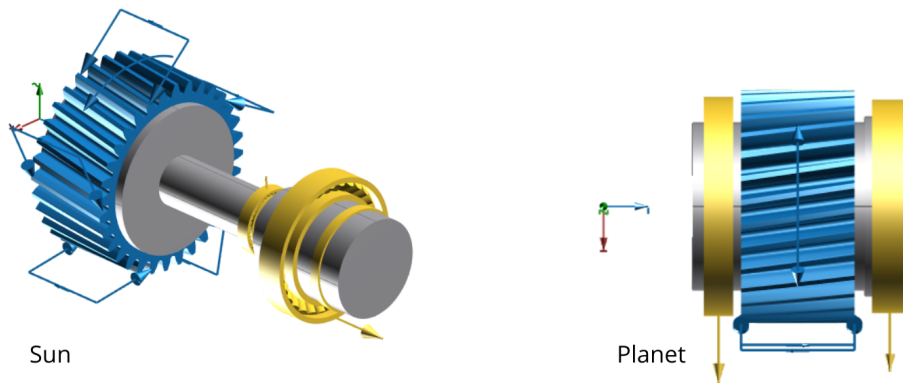


Figure A.5: Stage 1, final configuration design.

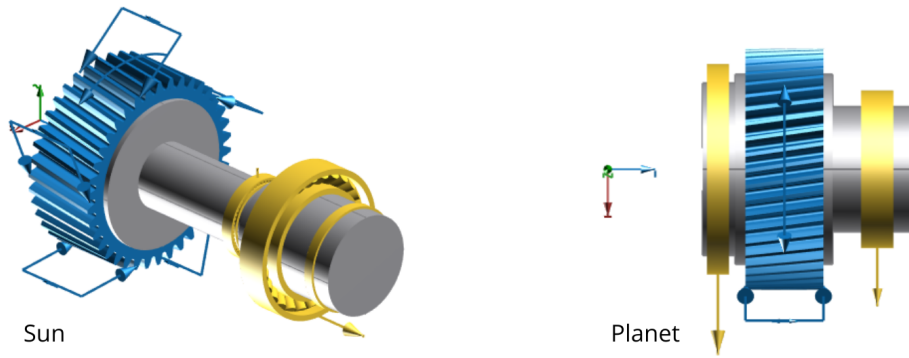


Figure A.6: Stage 2, final configuration design.

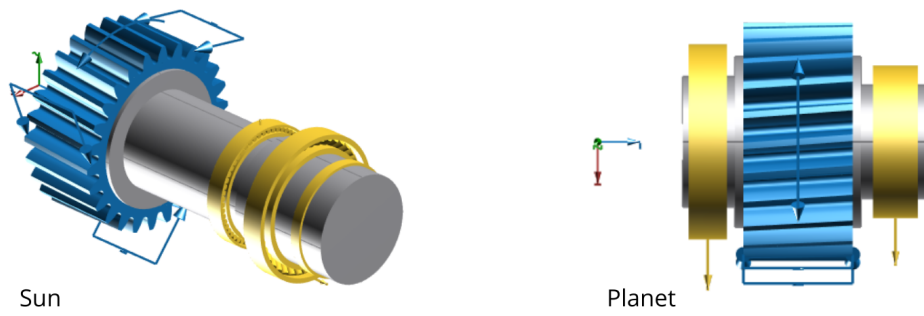


Figure A.7: Stage 3, final configuration design.

Bibliography

- [1] *Energy Statistic - an overview.*
https://ec.europa.eu/eurostat/statistics-explained/index.php?title=Energy_statistics_-_an_overview#Primary_energy_production (cit. on pp. 2, 3).
- [2] *What Is Climate Change.*
<https://climate.nasa.gov/what-is-climate-change/> (cit. on p. 2).
- [3] *Breve storia dell'energia eolica: all'origine della via del vento.*
<https://www.tuttogreen.it/breve-storia-dell%E2%80%99energia-eolica-all%E2%80%99origine-della-via-del-vento/> (cit. on p. 4).
- [4] Katinka Johansen. «Blowing in the wind: A brief history of wind energy and wind power technologies in Denmark». In: *Energy Policy* 152 (2021), p. 112139. ISSN: 0301-4215. DOI: <https://doi.org/10.1016/j.enpol.2021.112139>. URL: <https://www.sciencedirect.com/science/article/pii/S0301421521000082> (cit. on p. 4).
- [5] *What is offshore wind and what does its future look like?*
<https://www.weforum.org/agenda/2022/11/offshore-wind-farms-future-renewables/> (cit. on p. 5).
- [6] *Offshore Wind by Equinor.* <https://www.equinor.com/energy/offshore-wind> (cit. on p. 5).
- [7] *Explainer: What is offshore wind and what does its future look like.*
<https://www.weforum.org/agenda/2022/11/offshore-wind-farms-future-renewables/> (cit. on p. 5).
- [8] *Guided Tour on Wind Energy.*
<http://xn--drmsttre-64ad.dk/wp-content/wind/miller/windpower%20web/en/tour/> (cit. on pp. 8, 10, 11).
- [9] Dag Myrhaug. *Kompendium: Oceanography, Wind and Waves.* Nardoveien 12, Trondheim: Akademika, NTNU, 2006 (cit. on p. 12).
- [10] Martin O. L. Hansen. *Aerodynamics of Wind Turbines Second Edition.* 8–12 Camden High Street: y Earthscan, 2008 (cit. on pp. 14, 15, 19, 20).

-
- [11] *IEC 61400-1*. BSI Standards Limited. Wind energy generation systems - Part 1: Design requirements. The British Standards Institution, Apr. 2019 (cit. on pp. 20, 28).
- [12] *IEC 61400-3-1*. BSI Standards Limited. Wind energy generation systems - Part 3-1: Design requirements for fixed offshore wind turbines. The British Standards Institution, Sept. 2019 (cit. on pp. 21, 26).
- [13] *OpenFAST*. <https://www.nrel.gov/wind/nwtc/openfast.html> (cit. on p. 22).
- [14] M. Sirigu, E. Faraggiana, A. Ghigo, and G. Bracco. «Development of MOST, a fast simulation model for optimisation of floating offshore wind turbines in Simscape Multibody». In: *Journal of Physics: Conference Series* 2257.1 (Apr. 2022), p. 012003. DOI: 10.1088/1742-6596/2257/1/012003. URL: <https://dx.doi.org/10.1088/1742-6596/2257/1/012003> (cit. on p. 22).
- [15] *HAWC2*. <https://www.hawc2.dk/about-hawc2> (cit. on p. 22).
- [16] *Task 37 IEA Wind TCP*. <https://iea-wind.org/task37/> (cit. on p. 26).
- [17] Shuaishuai Wang, Amir R. Nejad, and Torgeir Moan. «Design and Dynamic Analysis of a Compact 10 MW Medium Speed Gearbox for Offshore Wind Turbines». In: *Journal of Offshore Mechanics and Arctic Engineering* 143 (June 2021). DOI: 10.1115/1.4048608 (cit. on p. 27).
- [18] Amir R. Nejad, Zhen Gao, and Torgeir Moan. «Long-term Analysis of Gear Loads in Fixed Offshore Wind Turbines Considering Ultimate Operational Loadings». In: *Energy Procedia* 35 (2013). DeepWind'2013 – Selected papers from 10th Deep Sea Offshore Wind RD Conference, Trondheim, Norway, 24 – 25 January 2013, pp. 187–197. ISSN: 1876-6102. DOI: <https://doi.org/10.1016/j.egypro.2013.07.172>. URL: <https://www.sciencedirect.com/science/article/pii/S1876610213012587> (cit. on p. 28).
- [19] *The Future of Wind Turbines: Comparing Direct Drive and Gearbox*. <https://www.engineering.com/story/the-future-of-wind-turbines-comparing-direct-drive-and-gearbox> (cit. on p. 30).
- [20] Farid K. Moghadam and Amir R. Nejad. «Evaluation of PMSG-based drivetrain technologies for 10-MW floating offshore wind turbines: Pros and cons in a life cycle perspective». In: *Wind Energy* 23.7 (2020), pp. 1542–1563. DOI: <https://doi.org/10.1002/we.2499>. URL: <https://onlinelibrary.wiley.com/doi/abs/10.1002/we.2499> (cit. on p. 30).
- [21] Yi Guo, T. Parsons, Katherine Dykes, and R.N. King. «A systems engineering analysis of three-point and four-point wind turbine drivetrain configurations: System Engineering Analysis of Drivetrain Designs». In: *Wind Energy* 20 (Aug. 2016). DOI: 10.1002/we.2022 (cit. on p. 30).

- [22] *Winergy website*. <https://www.winergy-group.com/en/products/gearboxes> (cit. on p. 30).
- [23] Shuaishuai Wang, Amir R. Nejad, and Torgeir Moan. «On design, modeling, and analysis of a 10-MW medium-speed drivetrain for offshore wind turbines». In: *Wind Energy* 23.4 (2020), pp. 1099–1117. DOI: <https://doi.org/10.1002/we.2476>. eprint: <https://onlinelibrary.wiley.com/doi/pdf/10.1002/we.2476>. URL: <https://onlinelibrary.wiley.com/doi/abs/10.1002/we.2476> (cit. on p. 31).
- [24] *Gear Train Internal Dynamics in Large Offshore Wind Turbines*. Vol. Volume 3: Advanced Composite Materials and Processing; Robotics; Information Management and PLM; Design Engineering. Engineering Systems Design and Analysis. July 2012, pp. 823–831. DOI: 10.1115/ESDA2012-83004. URL: <https://doi.org/10.1115/ESDA2012-83004> (cit. on p. 32).
- [25] *SKF website*. <https://www.skf.com/group/products/rolling-bearings/principles-of-rolling-bearing-selection/bearing-selection-process/bearing-type-and-arrangement/arrangements-and-their-bearing-types> (cit. on p. 35).
- [26] Amir Rasekhi Nejad, Yihan Xing, Yi Guo, Jonathan Keller, Zhen Gao, and Torgeir Moan. «Effects of floating sun gear in a wind turbine’s planetary gearbox with geometrical imperfections». In: *Wind Energy* 18.12 (2015), pp. 2105–2120. DOI: <https://doi.org/10.1002/we.1808>. URL: <https://onlinelibrary.wiley.com/doi/abs/10.1002/we.1808> (cit. on p. 48).